Article

Highly ordered clustering of TNFα and BAFF ligand-receptor-intracellular adaptor complexes on a lipid membrane

Chan Seok Lim [1], Jisun Lee[1], Ji Won Kim [2] & Jie-Oh Lee [1,2] ✉

The TNF family plays a critical role in immune regulation. Here, we present high-resolution structures of clusters formed by two TNF receptor family proteins, TNFR1 and BAFFR. Using a lipid monolayer method to mimic their membrane-bound state, we observe that the TNFα-TNFR1 complex forms highly ordered clusters of trimers on the lipid membrane. A non-competitive TNFR1 antagonist that inhibits receptor activation disrupted these clusters without blocking ligand binding or receptor trimerization. Furthermore, we find that the BAFF-BAFFR, BAFF-TACI, and BAFF-BCMA receptor-ligand complexes predominantly form pentagonal clusters of trimers on the lipid membrane. Notably, the binding of the intracellular adaptor TRAF3 to the BAFF-BAFFR complex induces a structural transition from a pentagonal to a flat hexagonal cluster. Mutations in BAFF that impair BAFFR activation prevented cluster formation. Our findings demonstrate that ligand binding induces the formation of highly ordered clusters of TNFR1 and BAFFR receptors on the lipid membrane, which is essential for their activation.

The tumor necrosis factor (TNF) family of proteins plays several critical roles in regulating immune responses, inducing apoptosis, regulating cell proliferation and differentiation, and maintaining tissue homeostasis[1]. Humans possess 19 TNF family ligands and 29 TNF receptor family members[2,3]. The binding of TNF family ligands to their specific receptors leads to the activation of transcription factors, such as NF-κB and AP-1, which can regulate gene expression and promote various cellular responses. TNF family ligands and receptors are among the most important targets for drug discovery[4]. For example, antibodies against TNFα, including adalimumab, named Humira commercially, are among the most successful protein-based drugs for reducing inflammation associated with several autoimmune diseases[5].

TNFα is the prototypical member of the TNF ligand family that can bind to two receptors, namely TNFR1 and TNFR2[6]. The structures of TNFα bound to the extracellular domain of TNFR1 have been elucidated using X-ray crystallography[7,8]. In the crystal structure, TNFα is a trimer arranged as a triangular cone, with each molecule in contact with the other two. The extracellular domain of TNFR1 is an elongated molecule composed of four disulfide-containing motifs, known as

cysteine-rich domains (CRDs), each comprising approximately 40 amino acids[9]. The TNFα trimer binds to three receptor molecules, one at each of the three TNF monomer–monomer interfaces. The binding of the trimeric ligand induces receptor trimerization and activates downstream signaling pathways by recruiting adaptor proteins, including TRADD[10,11]. The binding of TNFα to TNFR2 recruits TRAF2 instead of TRADD and activates the NF-κB and JNK pathways[12–14].

BAFF is a member of the TNF-ligand family. It promotes the survival and maturation of B cells and regulates the selection of the B cell repertoire[15–17]. BAFF expression is elevated in autoimmune diseases and serves as a therapeutic target for the treatment of systemic lupus erythematosus[18]. Soluble BAFF exists in two forms. Similar to other members of the TNF family, BAFF forms a trimeric complex in solution. Under certain conditions, BAFF trimers oligomerize to form a cage-like structure composed of 60 subunits[19,20]. A loop region, termed the "flap", facilitates the formation of the BAFF cage[19–22]. This oligomerization enhances BAFF's potency in promoting B cell survival and maturation. BAFF has three receptors, namely BAFFR, TACI, and BCMA, which contain one or two CRDs in their extracellular

[1]Department of Life Sciences, POSTECH, Pohang, Gyungbuk 37673, Korea. [2]Institute of Membrane Proteins, POSTECH, Pohang, Gyungbuk 37673, Korea. ✉e-mail: jieoh@postech.ac.kr

domains[23–25]. These receptors share substantial structural similarities and bind BAFF with high affinity. Activated BAFFR, BCMA and TACI recruit several TRAFs, including TRAF3, which subsequently negatively regulates NF-κB function[26–28].

TRAF proteins play essential roles in the intracellular signal transduction of several receptor families, including TNF, IL-1, Toll-like and NOD-like receptors[29]. Upon receptor activation, TRAFs are directly or indirectly recruited to the intracellular domains of the receptors. They subsequently engage other signaling proteins, which ultimately activate transcription factors such as NF-κB and AP-1 to induce immune and inflammatory responses and confer protection from apoptosis. TRAF family proteins exhibit a modular structure characteristic of adaptor proteins that function as docking assembly links for structurally dissimilar factors[30,31]. The C-terminal half of TRAF binds to receptors when activated. It can be further divided into two sections: the coiled-coil and TRAF-C domains. The coiled-coil domain folds into a parallel and triple coiled-coil structure, which enables the trimerization of TRAF proteins. The TRAF-C domain directly binds to the intracellular domains of the receptor[32–34]. The N-terminal half of TRAF proteins is more divergent, although all TRAF proteins except TRAF1 feature several zinc-finger domains. The N-terminal regions of TRAF2 and 6 dimerize both in solution as well as their crystal structures[35,36]. It has been proposed that they cross-link the trimeric C-terminal regions, inducing the formation of an extensive hexagonal network of TRAF proteins[37].

Previous studies have proposed that the trimeric TNFα-TNFR1 and BAFF-BAFFR complexes form higher-order aggregates[1,19,20,38–40]. However, high-resolution structures of these aggregates have not yet been reported, partly because the membrane-bound state of the receptor complexes could not be reproduced in X-ray crystallographic or cryo-electron microscopy (cryo-EM) studies using truncated or detergent-solubilized receptors. To overcome this technical hurdle, we employ a lipid monolayer method to mimic the membrane-anchored state of the proteins[41]. Using this approach, we successfully determine the clustered structures of the TNFα-TNFR1 and BAFF-BAFFR complexes at 3.3 Å resolution. Our results show that trimeric TNFα-TNFR1 units assemble into several highly ordered clusters with binary, bent, trigonal, linear quadruple, and quintuple arrangements. Similarly, trimeric BAFF-BAFFR complexes form ordered pentagonal, double-pentagonal, and half-spherical clusters on the membrane. Additionally, we demonstrate that TRAF3 binding induces a structural rearrangement of the pentagonal BAFF-BAFFR cluster, shifting it into a flat hexagonal configuration.

Results

Lipid monolayer method

Membrane receptors function while being attached to two-dimensional lipid membranes, and the lipid layer can significantly influence their structure and dynamics. Therefore, studying these receptors in their membrane-bound state is essential for understanding their ligand-binding and activation mechanisms. To achieve this, we adopted the lipid monolayer method[41]. The lipid monolayer method has been used to generate two-dimensional protein crystals for electron crystallographic studies and to concentrate samples on EM grids for affinity grid preparation[42]. In this approach, the hydrophobic fatty acid chains of the lipid layer face the air, while the hydrophilic head groups align toward the aqueous solution. We used a phospholipid monolayer containing 2–20% 18:1 DGS-NTA(Ni^{2+}) phospholipids to anchor hexa- or octa-histidine-tagged receptors to the lipid layer (Supplementary Fig. 1a). The histidine tag binds to the Ni-NTA head group, securing the receptor complexes to the lipid layer (Fig. 1a). After protein binding, the lipid monolayer was transferred onto a cryo-EM grid and imaged (Supplementary Fig. 1a). The lipid monolayer confines receptor complexes within the two-dimensional membrane, restricting their movement and facilitating lateral

interactions among the proteins. Compared to other artificial lipid layers that mimic cellular membranes—such as liposomes, bicelles, or nanodiscs[43]—the lipid monolayer offers a key advantage: it creates a large, flat membrane containing only a single lipid layer. This reduces background noise from the lipid layer and greatly simplifies cryo-EM analysis. In contrast, liposomes, bicelles, and nanodiscs contain lipid bilayers, where protein clusters can form on both sides of the membrane. Deconvoluting images of these heterogeneous clusters with varying sizes and shapes presents a significant challenge in structural analysis.

Clustering of the TNFα-TNFR1 ectodomain complex on the lipid membrane

To anchor the receptor to the lipid membrane containing 20% Ni-NTA lipids, an octa-histidine tag was fused to the C-terminus of the ectodomain of TNFR1, termed TNFR1ecto (Fig. 1a, Supplementary Fig. 1b and Supplementary Table 1). Subsequently, the TNFα-TNFR1ecto complex was generated by mixing TNFR1ecto with soluble TNFα (Supplementary Fig. 2). After purification, the receptor-ligand complex was bound to the Ni-NTA lipid monolayer, as shown in Fig. 1a, and the structure was determined by cryo-EM at a resolution of 3.3 Å (Supplementary Table 2). Cryo-EM images of the complex revealed a clustered pattern (Fig. 1b). The 2D class averaged images of the protein particles showed four major classes of clusters. In the binary cluster, dimerized TNFR1 receptors bridged two trimeric TNFα-TNFR1ecto complexes, forming a linear structure containing six ligands bound to receptors in a 1:1 molar ratio (Fig. 1c). This binary cluster served as the basic unit for the formation of larger clusters. In the bent cluster, two TNFR1 receptors in the central trimer formed dimeric interactions with TNFR1 receptors from the neighboring TNFα-TNFR1 trimeric units (Supplementary Fig. 3). In the trigonal cluster, three binary clusters were assembled around a central TNFα-TNFR1ecto trimer. A linear quadruple cluster was formed by connecting two binary clusters. Among these various clusters, the bent cluster, containing nine ligands and nine receptors, was the most abundant, comprising 42.8% of the total protein clusters.

To assess the effect of protein crowdedness on TNFα-TNFR1 clustering, we first varied the concentration of Ni-NTA lipids in the lipid layer. As shown in Supplementary Fig. 4, reducing the Ni-NTA lipid concentration from 20% to 2% resulted in no noticeable changes in either the number of protein particles on the membrane or their clustering pattern. However, decreasing the protein concentration in the monolayer preparation chamber from 1 mg/ml to 0.01 mg/ml facilitated the formation of larger clusters (Supplementary Fig. 5). At a protein concentration of 0.01 mg/ml, the proportions of binary and bent clusters decreased from 25% to 10% and from 50% to 8%, respectively. In contrast, the proportion of linear quadruple clusters increased by approximately sixfold. Additionally, 16% of the protein particles formed quintuple clusters, which were not observed under higher protein concentration conditions. The quintuple cluster consists of one additional TNFα-TNFR1 trimeric unit added to the linear quadruple cluster (Supplementary Fig. 6). We believe that the formation of clusters larger than the quintuple arrangement is highly unlikely due to the twisted nature of the binary cluster units (Fig. 2).

Dimerization between two TNFR1 receptors in neighboring trimeric units mediates the formation of all clusters (Fig. 2a). The TNFR1 dimer interface structures are identical across all cluster forms and can be divided into two distinct regions. The first dimer interface, previously referred to as the "PLAD" region in the literature, is primarily formed by CRD1 of TNFR1 (Supplementary Fig. 7a)[44]. A network of ionic bonds involving K19, H34, K35, D49, and E64 plays a major role at this CRD1 interface. Mutations of K19 or K32 to alanine have been shown to disrupt receptor dimerization[40,44]. In the structure, K19 is directly involved in receptor dimerization, whereas K32 contributes indirectly by stabilizing the CRD1 structure through its interaction with E64. The
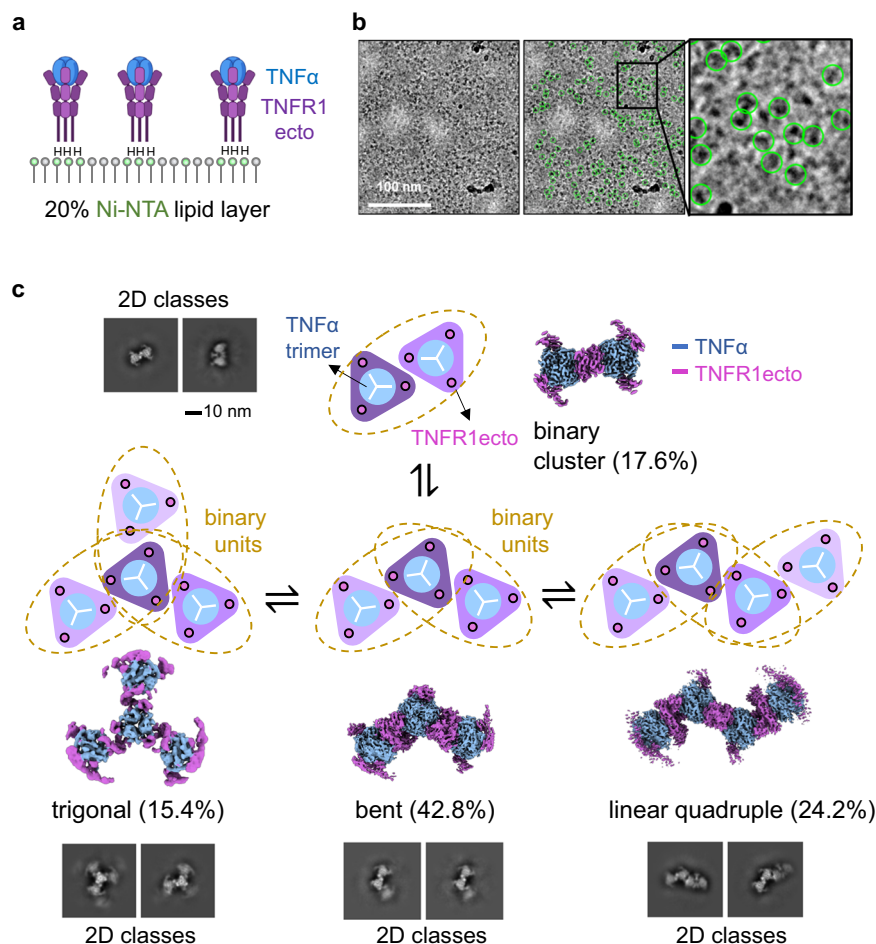
Fig. 1 | The TNFα-TNFR1ecto complex forms ordered clusters on the lipid layer. **a** An octa-histidine tag was attached to the C-terminus of TNFR1ecto, allowing the TNFα-TNFR1ecto complex to bind to the Ni-NTA lipid monolayer. The head groups of Ni-NTA lipids are indicated in green. "H" denotes the octa-histidine tag. Created in BioRender. Lim, C. (2025) https://BioRender.com/z6b5t4x. **b** A representative (n = 2,538) cryo-electron microscopy (cryo-EM) image of the TNFα-TNFR1ecto complex (left). Protein particles used for structure determination are highlighted with green circles (middle and right panels). **c** 2D class averages (left), a schematic diagram (middle), and a 3D refined map (right) of the binary cluster. Below are schematic diagrams, 3D refined maps, and 2D class averages of higher-order clusters formed by the assembly of the binary cluster units indicated by dashed orange circles. The proportion of protein particles belonging to each cluster is indicated in parentheses. The lipid layer consisted of 20% DGS-NTA(Ni²⁺) and 80% POPC.

second interface is formed by CRD4 of TNFR1. Here, ionic interactions between E131 and K132, hydrogen bonds between the two Q133 residues, and hydrophobic interactions involving L127 and V136 play key roles in dimer stabilization. Q130 and H126 are located in the contact region but do not appear to make strong interactions. Notably, the TNFα ligands are not directly involved in cluster formation.

The dimerization of TNFR1 was previously reported using X-ray crystallographic analysis[39]. They determined the structure of the TNFR1 ectodomain in the absence of bound ligands. This dimeric receptor structure is clearly an artifact of crystallization that cannot be reproduced in solution. However, notably, the dimeric structure of TNFR1ecto in the crystal state can be superimposed onto that of the binary cluster on the lipid membrane, showing a Cα r.m.s.d. of 1.7 Å (Supplementary Fig. 7b).

Clustering of the full-length TNFR1-TNFα complex on the lipid membrane

We produced a full-length TNFR1 receptor, named TNFR1fl (Supplementary Fig. 1b and Supplementary Table 1), to evaluate whether the transmembrane or intracellular domain of TNFR1 is involved in the clustering of the TNFα-TNFR1 complex and determined the TNFα-TNFR1fl complex structure (Supplementary Table 3). We fused a hexa-histidine tag to the C-terminus of the ligand and bound the

receptor–ligand complex to the Ni-NTA lipid monolayer (Fig. 2c and Supplementary Table 1). The 2D class averages of the cryo-EM images show that the TNFα-TNFR1fl complex formed the binary and bent clusters with a similar structure to those of the TNFα-TNFR1ecto complex (Supplementary Fig. 8). The cryo-EM map of the binary TNFα-TNFR1fl cluster was reconstituted at a resolution of 6.0 Å (Supplementary Table 3). The transmembrane and intracellular domains were not clearly visible in the map, presumably because of the structural flexibility of the connecting sequences between the extracellular, transmembrane, and intracellular domains (Fig. 2d and Supplementary Fig. 8). The binary cluster structures of the ectodomain and full-length TNFR1-TNFα complexes were practically identical, and the two structures could be superimposed with a Cα r.m.s.d. of 0.416 Å (Fig. 2e). This observation highlights that the extracellular domain of the receptor plays a major role in clustering and that the intracellular and transmembrane domains have minimal contributions, if any, to cluster formation. Trigonal, linear quadruple and quintuple clusters were not observed for the TNFα-TNFR1fl complex. This could be attributed to the small amount of detergent present in the buffer used to solubilize the full-length receptors. This detergent may have weakened the interactions between the receptors. Alternatively, this could be because the receptors are not directly attached to the lipid membrane and may have increased mobility, which destabilizes larger clusters (Fig. 2c).
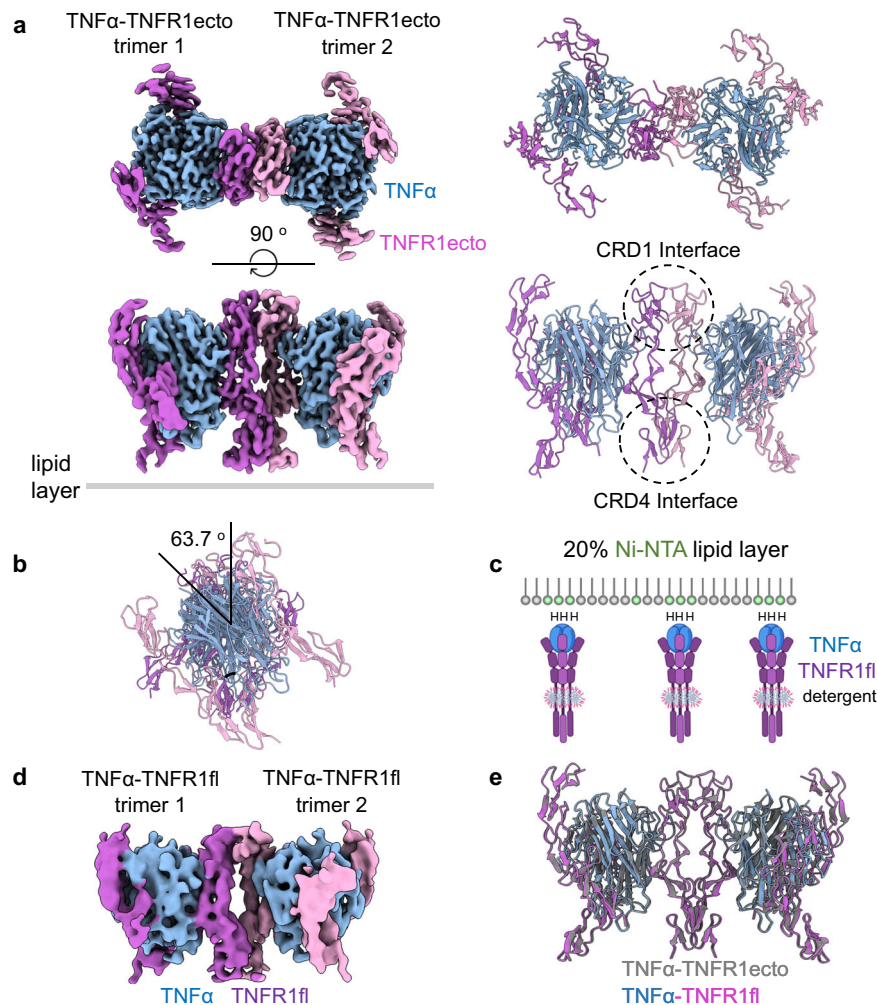
Fig. 2 | Structures of the binary clusters of the TNFα-TNFR1ecto and TNFα-TNFR1fl complexes. a Cryo-EM electron density map (left) and overall structure (right) of the binary cluster of the TNFα-TNFR1ecto complex. TNFα is colored blue, while TNFR1ecto in trimer 1 is dark purple and in trimer 2 is light purple. **b** The two TNFα-TNFR1ecto trimers are twisted by 63.7° when viewed from the side. **c** Tethering of the TNFα-TNFR1fl complex to the Ni-NTA lipid monolayer. A hexa-histidine tag was attached to the C-terminus of TNFα. Detergent belts are schematically represented in gray and purple. The head groups of Ni-NTA lipids are indicated in green. "H" denotes the histidine tag. Created in BioRender. Lim, C. (2025) https://BioRender.com/z6b5t4x. **d** Cryo-EM electron density map of the binary cluster of the TNFα-TNFR1fl complex. TNFα is colored blue, while TNFR1ecto in trimer 1 is dark purple and in trimer 2 is light purple. **e** Structural comparison of the binary clusters of the TNFα-TNFR1ecto and TNFα-TNFR1fl complexes. The TNFα-TNFR1ecto complex is shown in gray, while TNFα and TNFR1fl in the TNFα-TNFR1fl complex are colored blue and purple, respectively.

Disruption of TNFα-TNFR1 clusters by a non-competitive antagonist

DOM1h-574-208 is a nanobody that has been shown to inhibit TNFR1 receptor activation without disrupting TNFα binding[45]. It significantly reduces IL-8 production induced by TNFα in HEK293 cells transfected with TNFR1[46]. The long-lasting variant of DOM1h-574-208, named DMS5541 or TNFR1-AlbudAb, has demonstrated effectiveness in KYM-1D4 cell cytotoxicity assays and in the dose-dependent upregulation of VCAM-1 in HUVECs[47]. Additionally, it reduces osteoclast formation in ex vivo human rheumatoid synovial membrane cell cultures[48]. However, the precise mechanism of action of this non-competitive antagonist remains unclear. To elucidate the structural basis of DOM1h-574-208-mediated antagonism, we determined the structure of the TNFα-TNFR1ecto-DOM1h-574-208 complex in both solution and lipid-bound states (see below and Supplementary Table 3). The solution-state structure revealed that the DOM1h nanobody binds to the CRD4 region of TNFR1 (Fig. 3a). In this structure, the TNFα-TNFR1ecto complex retains its 3:3 assembly, with the trimeric ligand bound to three receptors. We did not observe any clustered structures of the receptor-ligand-nanobody complex. The 2D class-averaged

images clearly show that the nanobody binds to the CRD4 region of TNFR1 in a 1:1 ratio (Fig. 3b, c), although some 2D class images show partial occupancy of the three nanobody binding sites, likely due to the nanobody's low affinity. To enhance the resolution, we performed focused refinement using an envelope encompassing the CRD4 region of TNFR1 and the nanobody (See Methods for details). The structure shows that the nanobody binding site is positioned opposite to the ligand-binding site, ensuring that ligand binding and receptor trimer-ization remain undisturbed. Our cryo-EM structure and the molar ratio observed for the TNFα−TNFR1−DOM1h nanobody complex are consistent with those previously reported in a U.S. patent, determined at 2.9-Å resolution by X-ray crystallography[49].

In the membrane-bound state, we found that DOM1h binding weakened TNFR1-TNFR1 dimeric interactions, leading to the dissolution of approximately 60% of receptor clusters into isolated TNFα-TNFR1ecto trimeric units (Fig. 3c). The remaining 40% of nanobody-bound proteins exhibited a distorted binary structure. The cryo-EM map of this binary cluster clearly demonstrated that the nanobody disrupts the CRD4 interface of the TNFR1 dimer, causing the two tri-meric TNFα-TNFR1 units to rotate by approximately 60° compared to
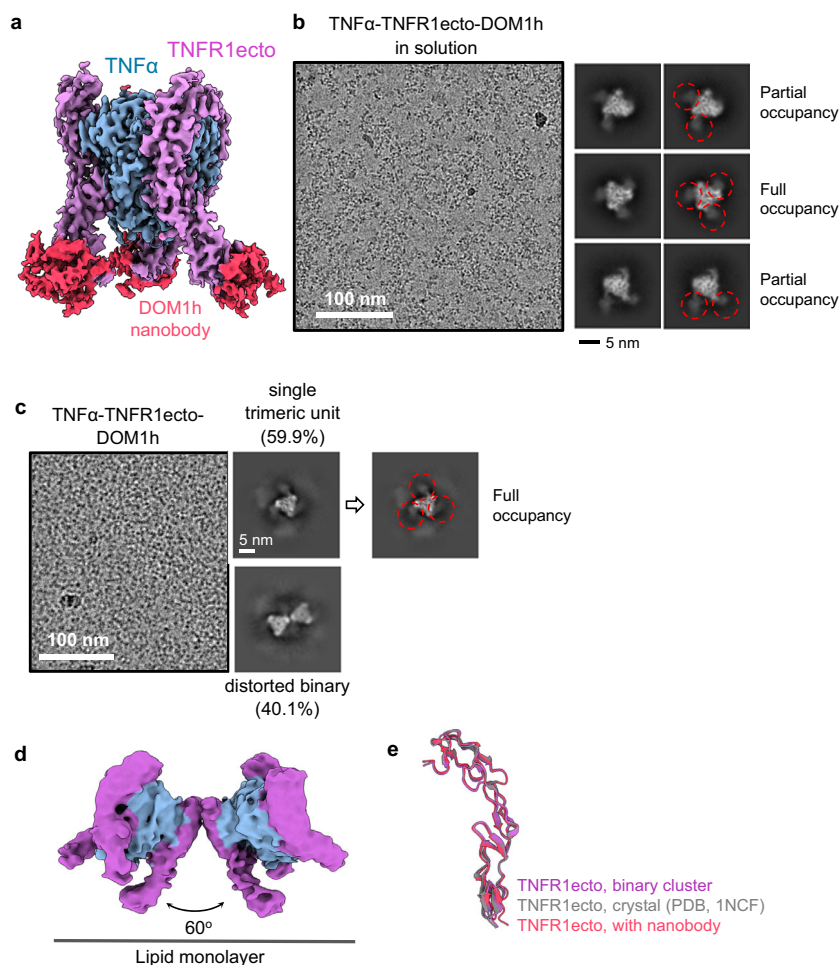
Fig. 3 | The DOM1h-574-208 nanobody disrupts the ordered binary cluster of the TNFα-TNFR1ecto complex. a Composite electron density map of the TNFα-TNFR1ecto-DOM1h nanobody complex in solution. TNFα, TNFR1ecto, and DOM1h are shown in blue, purple, and red, respectively. Focused refinement was performed on one of the three DOM1h nanobody regions in the map, after which maps for the remaining two nanobodies were generated by applying threefold symmetry. **b** Representative (*n* = 6408) image (left) and 2D class averages (middle) of the TNFα-TNFR1ecto-DOM1h nanobody complex in solution. The electron densities correspond to the bound nanobodies are highlighted with dashed red circles on the right panel. **c** Representative (*n* = 634) image (left) and 2D class averages (middle) of the TNFα-TNFR1ecto-DOM1h nanobody complex bound to the lipid monolayer. The proportion of protein particles belonging to each cluster is indicated in parentheses. The electron densities correspond to the bound nanobodies are highlighted with dashed red circles on the right panel. **d** Cryo-EM electron density map of the distorted binary cluster of the TNFα-TNFR1ecto-DOM1h nanobody complex bound to the Ni-NTA lipid layer. TNFα and TNFR1ecto are shown in blue and purple, respectively. **e** Superimposition of TNFR1ecto structures. TNFR1ecto in the ordered TNFα-TNFR1ecto binary cluster, the crystal structure, and the distorted TNFα-TNFR1ecto-DOM1h binary cluster are shown in purple, gray, and red, respectively.

the binary cluster without the nanobody (Fig. 3d). The nanobodies are not visible in this low-resolution map, presumably due to structural flexibility in the CRD4 region of the TNFR1 receptor. This cluster disruption was not due to structural changes in the receptor itself, as the receptor structures with and without the bound nanobody could be superimposed with a Cα r.m.s.d. of 0.684 Å (Fig. 3e). Our structural observations, together with the reported antagonistic activity of the DOM1h nanobody, demonstrate that proper clustering is essential for TNFα-mediated TNFR1 activation.

Clustering of the BAFF-BAFFR, BAFF-BCMA and BAFF-TACI complexes on the lipid membrane

To determine the structure of the BAFF-BAFFRecto complex in its membrane-bound state, an octa-histidine tag was fused to the C-terminus of the BAFFR ectodomain, termed BAFFRecto (Supplementary Fig. 1b and Supplementary Table 4). The BAFF-BAFFRecto complex was then formed by mixing BAFFRecto with BAFF. For this study, we used a soluble form of BAFF that lacks a transmembrane domain (Supplementary Fig. 1b and Supplementary Table 4). The

trimeric BAFF-BAFFRecto complex was purified and subsequently attached to the Ni-NTA lipid monolayer, as shown in Fig. 4a. The structure of the complex was then determined by cryo-EM at a resolution of 3.3 Å (Supplementary Table 5). When bound to the lipid monolayer, the BAFF-BAFFRecto complex, which is trimeric in solution, formed three distinct types of clusters (Fig. 4a, lower panels). The predominant form was a pentagonal cluster composed of five trimeric BAFF-BAFFRecto units (Fig. 4b). However, a significant number of double pentagons and half-spherical structures were also observed. The double pentagonal cluster resulted from the fusion of two pentagonal clusters, while the fusion of three pentagonal clusters led to the formation of a half-spherical BAFF-BAFFRecto cluster. Notably, no particles corresponding to a fully assembled globular cage-like structure of the BAFF-BAFFRecto complex were observed.

The structure of the pentagonal cluster of BAFF-BAFFRecto was practically identical to the pentagonal substructure of the full-sized BAFF-BAFFRecto cage, and the two structures could be superimposed with a Cα r.m.s.d. of 1.17 Å (Supplementary Fig. 9, left panel). The double-pentagon and half-sphere cluster structures could be
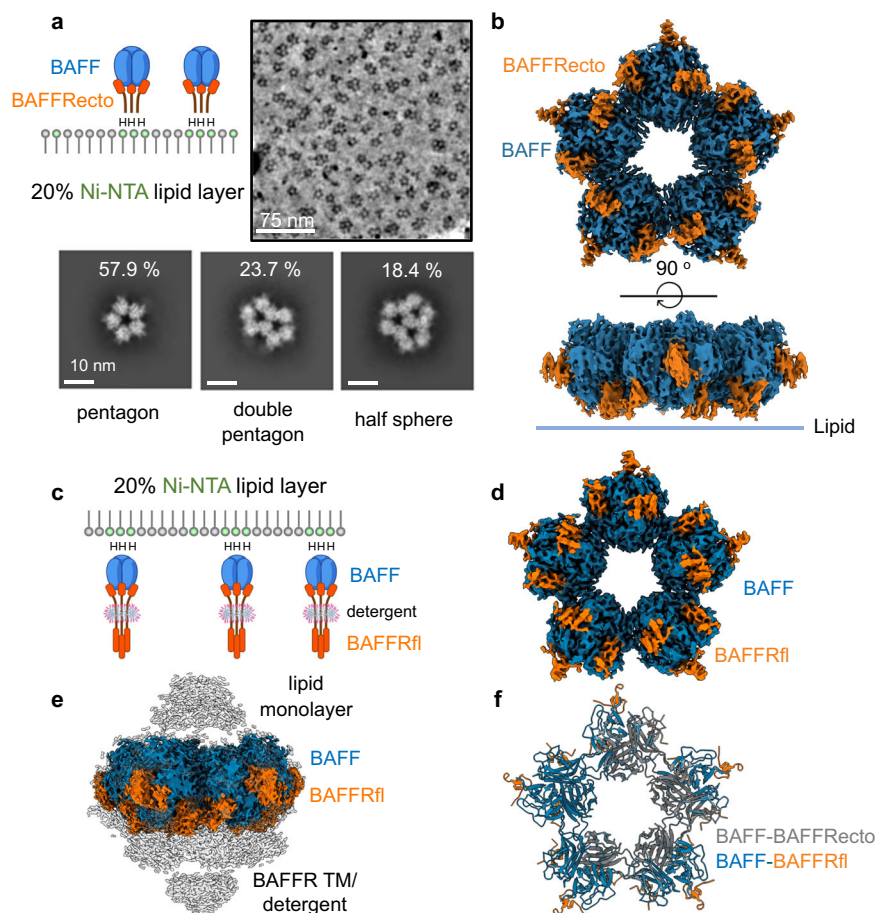
Fig. 4 | The BAFF-BAFFRecto complex forms ordered clusters on the lipid layer. **a** An octa-histidine tag was attached to the C-terminus of BAFFRecto, allowing the BAFF-BAFFRecto complex to bind to the Ni-NTA lipid monolayer. A representative ($n = 1464$) cryo-EM image (upper right) and 2D class averages (lower three panels) of the clusters are shown. The proportion of protein particles belonging to each cluster is written above the 2D class images. The head groups of Ni-NTA lipids are indicated in green. "H" denotes the histidine tag. Created in BioRender. Lim, C. (2025) https://BioRender.com/z6b5t4x. **b** Cryo-EM electron density map of the BAFF-BAFFRecto pentagonal cluster. BAFF and BAFFRecto are colored blue and orange, respectively. **c** A hexa-histidine tag was attached to the N-terminus of BAFF, enabling the BAFF-BAFFRfl complex to bind to the Ni-NTA lipid monolayer. Created in BioRender. Lim, C. (2025) https://BioRender.com/z6b5t4x. **d** Cryo-EM map of the pentagonal BAFF-BAFFRfl cluster. The maps for the BAFF and BAFFRfl proteins are colored blue and orange, respectively. The view is the same as in the upper panel of (**b**). **e** Cryo-EM maps of the BAFF-BAFFRfl cluster. The lower and higher contour level maps are colored gray and blue/orange, respectively. **f** Structural comparison of the pentagonal BAFF-BAFFRecto and BAFF-BAFFRfl clusters. The BAFF-BAFFRecto structure is shown in gray, while BAFF and BAFFRfl in the BAFF-BAFFRfl cluster are colored blue and orange, respectively.

superimposed onto the full-sized cage structure, albeit with significantly higher Cα r.m.s.d. values because the outer parts of the clustered structures shifted downwards toward the lipid membrane by approximately 20 Å (Supplementary Fig. 9, middle and right panels). It appears that the flattening of the cluster, which is necessary for the receptors to attach to the lipid membrane, was responsible for the structural differences. As a control, the full-sized cage form of BAFF was prepared by concentrating the protein sample above 1.5 mg/ml (Supplementary Fig. 10a). After purifying the BAFF cage, it was added to BAFFRecto, which had previously been bound to the lipid monolayer. The complex was then analyzed using cryo-EM. The analysis showed that approximately half of the BAFF cage disintegrated into the pentagonal cluster (Supplementary Fig. 10b and Supplementary Table 6). This finding demonstrates that the full-sized BAFF cage becomes unstable and transforms into the pentagonal cluster when bound to BAFFR attached to the lipid membrane.

We produced a full-length BAFFR, named BAFFRfl, to evaluate whether the transmembrane or intracellular domain of BAFFR induces structural changes in the BAFF-BAFFRecto clusters (Supplementary Table 4). A hexa-histidine tag was fused to the N-terminus of BAFF and the receptor-ligand complex was bound to the Ni-NTA lipid monolayer

(Fig. 4c). This mimics the membrane-bound form of BAFF because full-length BAFF contains a transmembrane domain at the N-terminus of soluble BAFF (Supplementary Fig. 1b). Both the membrane-bound and soluble forms of BAFF exhibit full biological activity[23,24]. The 2D class averages of the cryo-EM images revealed that the BAFF-BAFFRfl complex primarily formed a pentagonal cluster with a structure similar to that of the BAFF-BAFFRecto complex (Supplementary Fig. 11). The cryo-EM map corresponding to the transmembrane and intracellular domains of BAFF-BAFFRfl was not clearly visible, presumably because of the structural flexibility of the connecting sequences between the extracellular, transmembrane and intracellular domains (Fig. 4d, e). Structural differences between the pentagonal clusters of the ectodomain and full-length BAFFR-BAFF complexes were negligible, and the two structures could be superimposed with a Cα r.m.s.d. of 0.189 Å (Fig. 4f). These data demonstrate that BAFF bound to the extracellular domain of the receptor plays a major role in the clustering of the receptor-ligand complexes, whereas the intracellular or transmembrane domain of the BAFFR receptor has only minimal contributions, if any, to cluster formation.

To determine whether the pentagonal clustering of BAFF is conserved when bound to other BAFF receptors, we analyzed the
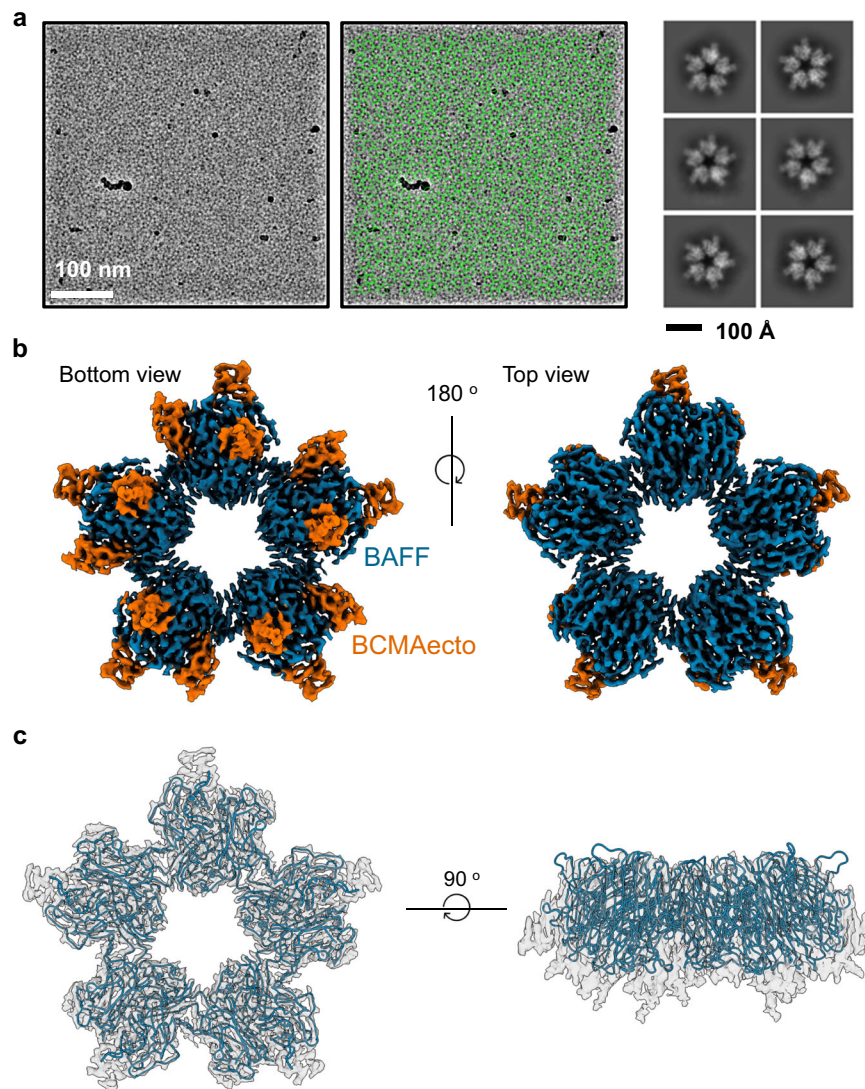
Fig. 5 | Cryo-EM structure of the BAFF-BCMAecto complex. a Representative (*n* = 1,571) cryo-EM micrograph (left) and 2D class averages (right) of the BAFF-BCMAecto complex. Protein particles selected for 3D map reconstruction are highlighted with green circles (middle panel). **b** 3D reconstructed map of the BAFF-BCMAecto complex, with an estimated resolution of 2.5 Å. The BAFF and BCMAecto maps are colored blue and orange, respectively. **c** 3D cryo-EM density map of the BAFF-BCMAecto complex. The structure of the BAFF cluster extracted from the pentagonal BAFF-BAFFRecto cluster is fitted into the map. The structure and density map are colored blue and gray, respectively. The BCMAecto structures are not shown.

structures of the BAFF-BCMAecto and BAFF-TACIecto complexes. Although the extracellular domains of BCMA and TACI share a homologous structure with BAFFR, their sequences exhibit substantial divergence (Supplementary Fig. 12). Residues exposed on the receptor surface that are not involved in ligand binding show significant sequence variations. To examine the structure of BCMA or TACI in their membrane-bound states, the receptor-ligand complexes were bound to the Ni-NTA lipid monolayer and imaged using cryo-EM (Figs. 5 and 6). The 3D maps of the complexes were reconstructed at resolutions of 2.5 Å and 2.9 Å for BAFF-BCMAecto and BAFF-TACIecto, respectively (Supplementary Table 7). The structure of the pentagonal BAFF cluster formed by the BAFF-BAFFR complex fit well into the reconstructed EM maps without requiring significant structural adjustments, demonstrating that the clustered structure of BAFF is conserved in both BAFF-BCMAecto and BAFF-TACIecto complexes, despite sequence variations in the receptors. This finding confirms that pentagonal clustering is a conserved feature among all three BAFF receptors—BAFFR, BCMA, and TACI—when bound to BAFF on the lipid layer.

Disruption of BAFF-BAFFR clustering by mutations in the flap region

In solution, purified BAFF trimers can oligomerize to form a cage-like structure comprising 60 subunits[19,20]. The "flap" regions of BAFF mediate cage formation. We found that the assembly of the pentagonal cluster in the BAFF-BAFFRecto structure is also mediated by interactions between the flap regions of two BAFF trimers (Fig. 7a, Supplementary Fig. 13a). The BAFFR receptors do not participate in cluster formation. Strong ionic interactions between R214, K216, D222, and E223 of BAFF play a central role in this dimeric interaction. As shown in Supplementary Fig. 13b, virtually no movement in the flap regions is required to induce a structural transition from the globular cage to the flat pentagonal cluster.

Previously, two mutations in the flap region, H242A and E247K, have been demonstrated to interfere with the biological activity of mouse BAFF without disrupting its binding to the BAFFR receptor[22]. The study revealed that these mutations blocked BAFF signaling in reporter cell assays, disrupted B-cell maturation in the spleen, and altered the B/T cell ratio in the lymph nodes of knock-in mouse
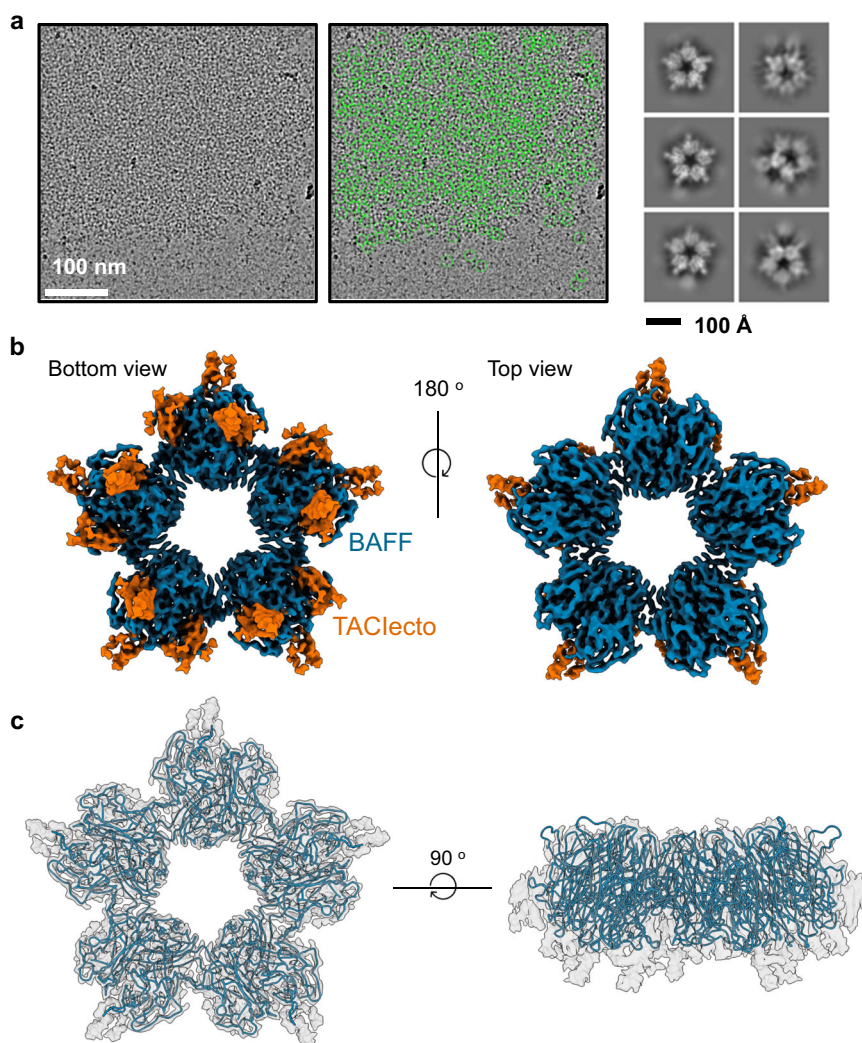
Fig. 6 | Cryo-EM structure of the BAFF-TACIecto complex. a Representative (*n* = 5302) cryo-EM micrograph (left) and 2D class averages (right) of the BAFF-TACIecto complex. Protein particles selected for 3D map reconstruction are highlighted with green circles (middle panel). **b** 3D reconstructed map of the BAFF-TACIecto complex, with an estimated resolution of 2.9 Å. The BAFF and TACIecto maps are colored blue and orange, respectively. **c** 3D cryo-EM density map of the BAFF-TACIecto complex. The structure of the BAFF cluster extracted from the pentagonal BAFF-BAFFRecto cluster is fitted into the map. The structure and density map are colored blue and gray, respectively. The TACIecto structures are not shown.

models. Among these, E247K exhibited the most significant inhibitory effect on BAFF function. H242 and E247 residues of mouse BAFF correspond to H218 and E223, respectively, in human BAFF. These mutations were introduced into the BAFF ligands to investigate whether they interfere with the formation of receptor-ligand clusters on the lipid layers and to determine the structure of the BAFF-BAFFRecto complex bound to the Ni-NTA lipid layer. The wild-type and mutant complex structures were observed using cryo-EM (Supplementary Table 6). Conservative K216R and H218A mutations with milder inhibitory effects partially disrupted the pentagonal clusters (Fig. 5b, c). However, for the E223K mutation, which exhibited the most severe inhibitory effect in mice, the ordered structure of the pentagonal cluster was completely disrupted, and consequently, disordered aggregates were formed. These data demonstrate that receptor clustering with a properly ordered structure is essential for the activation of BAFF signaling.

TRAF3 binding induces a structural shift in the BAFF-BAFFRfl cluster

We conducted a lipid monolayer experiment using soluble BAFF, full-length BAFFR, and TRAF3 to explore the effects of TRAF3 binding to the BAFF-BAFFRfl cluster (Supplementary Table 8). The N-terminal RING and Zinc finger domains, which are dispensable for receptor binding, were removed from TRAF3 (Supplementary Fig. 1b). For membrane attachment, the BAFF ligand was tagged with a hexa-histidine sequence at the N-terminus and mixed with detergent-solubilized full-length BAFFR (Fig. 8a). In this section, the histidine-tagged BAFF is renamed hisBAFF to emphasize the position of the tag for clarity (Supplementary Table 4). After forming the hisBAFF-BAFFRfl complex, TRAF3 was added to the mixture, and the complex structure bound to the lipid monolayer was determined by cryo-EM at a resolution of 3.8 Å (Supplementary Table 8).

Previous crystallographic studies have shown that the trimerized coiled-coil domain of TRAF3 extends as long rod-like structures. This coiled-coil rod served as a convenient landmark for analyzing the TRAF3 cluster, as it appeared as a bright white dot in the cryo-EM 2D class averages (Supplementary Fig. 14a). As shown in Fig. 8b, c, the hisBAFF-BAFFRfl-TRAF3 complex formed a large, flat hexagonal lattice. Due to the structural flexibility of the sequences linking the extracellular, transmembrane, and intracellular domains of the receptor, only the short intracellular tail of BAFFR, consisting of 17 amino acids bound to TRAF3, was clearly visible in the map. The structure of the

BAFFR intracellular domain within the cluster closely resembled the crystal structure of the BAFFR intracellular peptide bound to the TRAF3 trimer, with the two structures superimposing at a Cα r.m.s.d. of 1.27 Å (Supplementary Fig. 14b).

The electron density map for the extracellular portion of the BAFF−BAFFR complex was only partially visible, presumably due to structural flexibility in the sequences connecting the receptor domains. This low-resolution map revealed a trigonal arrangement of BAFF−BAFFR trimers (Fig. 8d, e). We hypothesize that TRAF3 binding induces a structural shift toward the hexagonal cluster. However, the symmetric arrangement on the extracellular side of the BAFF−BAFFR complex is imperfect and becomes indistinct during cryo-EM map averaging, leaving only a trigonal subset of the hexagonal cluster visible in the EM map. Unexpectedly, we observed additional TRAF3 helical rods, depicted as gray densities in Fig. 8b, c, and Supplementary Fig. 14c, intercalating within the hexagonal lattice in an inverted orientation. This additional TRAF3 layer is likely an artifact resulting from TRAF3 truncation, as in full-length TRAF3, the N-terminal zinc finger domains prevent the intercalation of a second TRAF3 layer (Supplementary Fig. 1b).

To further confirm the structural shift induced by TRAF3 binding, we relocated the histidine tag from the ligand to the N-terminus of TRAF3 (Fig. 8f and Supplementary Table 4) and determined the complex structure using cryo-EM (Supplementary Table 8). The histidine-tagged TRAF3 was designated hisTRAF3 to emphasize the position of the tag (Supplementary Table 4). As expected, cryo-EM images and 2D class averages revealed a hexagonal TRAF3 lattice (Supplementary Fig. 14d). The 3D reconstructed map also showed a hexagonal TRAF3-BAFFR intracellular domain cluster (Fig. 8g, h). The structure of the BAFF-BAFFRfl-hisTRAF3 cluster was nearly identical to that of hisBAFF-BAFFRfl-TRAF3, with the two structures superimposing at a Cα r.m.s.d. of 1.17 Å (Supplementary Fig. 14e). The extracellular portion of the BAFF-BAFFRfl-hisTRAF3 complex was not visible, likely due to the structural flexibility of the linkers connecting the BAFFR domains and the lower resolution of this map compared to that of the hisBAFF-BAFFR-TRAF3 complex. Notably, no second TRAF3 layer was observed in this structure (Fig. 8g, h, and Supplementary Fig. 14f). This structural observation confirms that hexagonal clustering is driven by TRAF3 binding to BAFF-BAFFR and that the second TRAF3 layer observed in Fig. 8b, c had no effect on BAFF-BAFFR-TRAF3 cluster formation.

The TRAF-C and BAFFR intracellular domains mediate the clustering of the BAFF-BAFFR-TRAF3 complex. The coiled-coil domains of TRAF3 are separated by 72.6 Å within the cluster and do not contribute to its formation (Fig. 8c, h). P164″, A165″, and T166″ of BAFFR, T469 and H470 in the first TRAF3 trimer, and D463′, F474′, and P535′ in the second TRAF3 trimer make close contact within the cluster (Fig. 9a, b). Three M465 side chains of the TRAF3 trimers are positioned at the center of the TRAF3 cluster, forming a small hydrophobic core. Additionally, we found that T541 and N545 in the first TRAF3 trimer, along with N517′, S518′, and S519′ in the second TRAF3 trimer, form a hydrogen-bonding network that stabilizes the TRAF3 cluster. However, these interactions appear weak compared to those in stable protein complexes, which may explain why BAFF-BAFFR-TRAF3 clustering cannot be reproduced in the absence of a bound lipid layer. Based on our structural observations, we propose a model for BAFFR receptor activation (Fig. 9c). The binding of trimeric ligands induces receptor trimerization. Subsequently, receptor-ligand trimers primarily form pentagonal clusters on the membrane. The binding of the intracellular adaptor TRAF3 to BAFFR induces a structural shift in the receptor cluster, resulting in a flat hexagonal lattice that initiates intracellular signaling.

Discussion

We used the lipid monolayer method to demonstrate that the TNFα-TNFR1 complex forms binary, bent, trigonal, linear quadruple, and quintuple clusters. We found that dimeric interactions between TNFR1 proteins in neighboring TNFα-TNFR1 trimers mediate cluster formation and that a non-competitive TNFR1 antagonist inhibits this process. Additionally, we observed that the BAFF-BAFFR complex forms pentagonal, double-pentagonal, and half-sphere clusters when attached to the lipid layer. TRAF3 binds to this cluster and induces a structural shift toward a flat hexagonal cluster. Furthermore, we found that BAFF mutations interfering with BAFFR intracellular signaling disrupt receptor clustering. These findings demonstrate that highly ordered TNFα-TNFR1 and BAFF-BAFFR clustering plays a crucial role in receptor activation.

The trimerization and expanding network hypotheses are two models proposed to explain how TNFR1 is activated upon binding to the TNFα ligand[38]. The trimerization hypothesis proposes that the juxtaposition of the three receptors, resulting from the binding of a single TNFα trimer, initiates cell signaling. In this model, the TNFα trimer binds to three receptor molecules, one at each of three TNF monomer-monomer interfaces. The trimerization of the receptors enhances the binding affinity of TRADD and other downstream adaptors to the receptors, ultimately activating signaling pathways[7]. In contrast, the expanding network hypothesis proposes that the binding of the TNFα trimer to preformed receptor dimers generates a hexagonal array of ligand-receptor complexes. In this model, each TNFα trimer engages three receptor dimers, subsequently triggering network expansion and biological responses. The expanding network hypothesis was proposed based on a crystallographic study of receptor dimers[39]. Our cryo-EM study with membrane-attached receptors provides the first high-resolution evidence demonstrating that the proposed network expansion hypothesis is essentially correct, although the network expansion is limited and the resulting cluster size is much smaller because of its twisted nature.

Our structural observations are consistent with the model proposed based on a single-molecule study using fluorescence microscopy. Recently, Karathanasis et al. employed quantitative, single-molecule super-resolution microscopy to directly study TNFR1 assembly in native cellular environments and at physiological cell surface abundance[40]. Using single-molecule localization microscopy combined with TIRF illumination, they determined the oligomeric state of TNFR1 and found that, in the absence of TNFα, TNFR1 exists as a mixture of monomers and dimers. Upon TNFα binding, TNFR1 aggregates into trimers and 9-mers. The oligomeric state of TNFR1 receptors before ligand binding cannot be determined by cryo-EM analysis because their monomeric or dimeric forms are too small. However, consistent with their fluorescence experiments, we observed that the bent cluster containing nine receptors is the most abundant cluster form when bound to the ligand, provided that the protein concentration on the lipid layer is sufficiently high (Supplementary Fig. 5). We found that at lower protein concentrations, more extended clusters, such as linear quadruple or quintuple clusters, are preferred. One possible explanation is that lower protein concentrations on the membrane provide more space for the formation of extended assemblies. We observed that the clustering interaction in the TNFα ligand-receptor complex does not resemble typical protein-protein interactions in solution. Rather, it is intrinsically weak, dynamic and cannot be readily reproduced in solution. Its formation probably involves a subtle balance between enthalpic and entropic contributions. A detailed computational analysis will be necessary to understand the mechanisms governing protein clustering states on the lipid membrane.

Previously, mutations in the flap region of BAFF have been shown to interfere with its biological activity without blocking ligand binding[50]. For example, purified BAFF with the flap region deleted maintained normal binding affinity to the BCMA receptor but failed to activate NF-κB in HEK293 cells transfected with the BCMA receptor gene[21]. Furthermore, this deletion mutant exhibited substantially
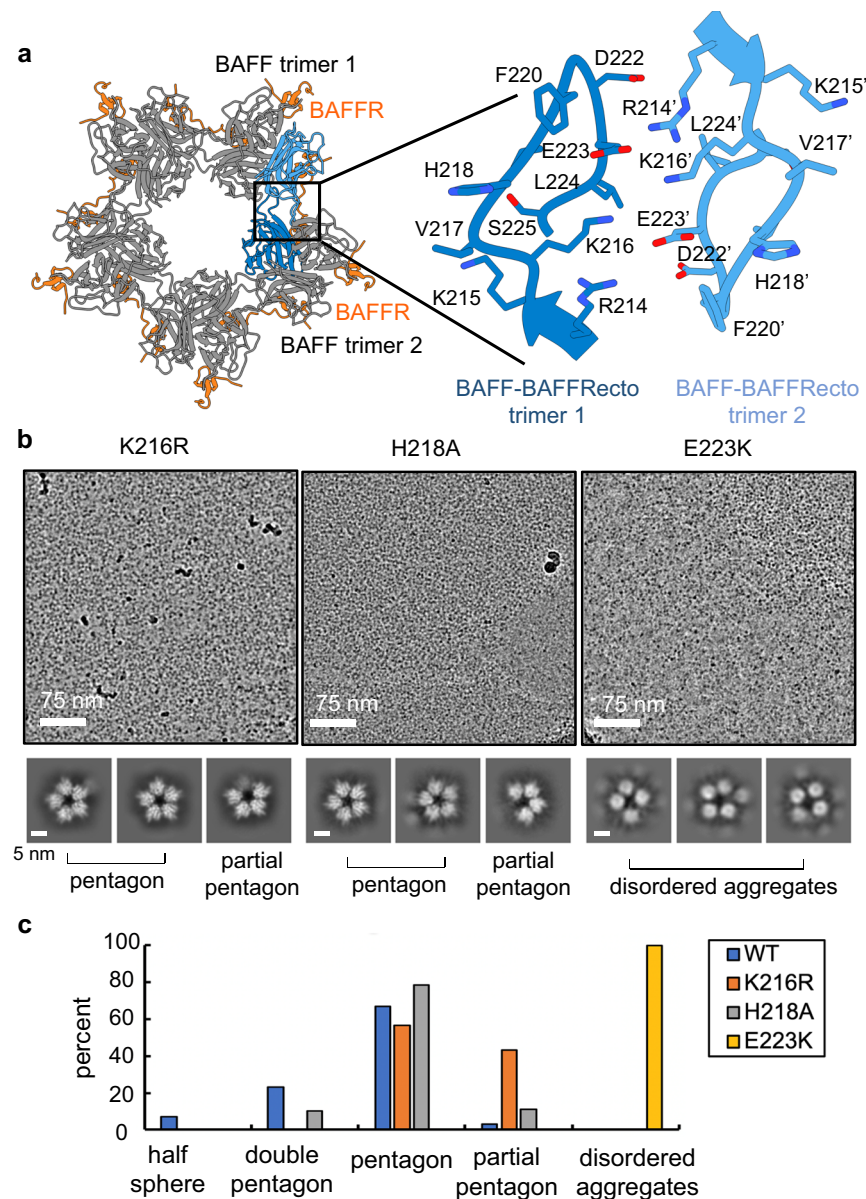
Fig. 7 | Mutations in the "flap" region of BAFF disrupt BAFF-BAFFRecto clusters. a Close-up view of the BAFF clustering interface in the BAFF-BAFFR pentagonal cluster. BAFF and BAFFR proteins are shown in gray and orange, respectively. Two BAFF proteins involved in clustering interactions are highlighted in light and dark blue, with a zoomed-in view provided in the right panel. Oxygen and nitrogen atoms in the side chains are colored red and dark blue, respectively. Residue numbers for BAFF and BAFFR in the second BAFF trimer are indicated with apostrophes. **b** Representative cryo-EM images (upper) and 2D class averages (lower three panels) of mutant BAFF-BAFFRecto complexes. Representative micrographs are from $n = 816$ (K216R), $n = 628$ (H218A) and $n = 581$ (E223K) cryo-EM experiment sets, respectively. **c** Histogram showing the proportions of each cluster in wild-type and mutant BAFF-BAFFRecto complexes.

reduced activity in stimulating B lymphocyte proliferation. In a subsequent study, two mutations in the flap region, H242A and E247K of mouse BAFF, were shown to interfere with the biological activity without affecting its binding affinity to the BAFFR receptor[22]. These mutant proteins retained normal binding affinity to BAFFR. Among these mutations, E247K exhibited the most significant inhibitory effect on BAFF function. Specifically, the study revealed that the E247K mutation, but not the H242A mutation blocked normal BAFF signaling in BAFFR-Fas reporter assays using transfected HEK293 cells and in cell viability assays using purified primary splenic B cells. This mutational effect in the flap region could be overcome by antibody-mediated cross-linking. Moreover, the E247K mutation disrupted B-cell maturation in the spleen and altered the B/T cell ratio in the lymph nodes of knock-in mouse models. In another study, the H218A mutation in human BAFF significantly inhibited B lymphocyte proliferation under

BCR-stimulating conditions[51]. The H218 residue in human BAFF corresponds to the H242 residue in mouse BAFF. Our structural study of the BAFF-BAFFR complex on the lipid layer demonstrates that the flap region mediates the formation of precisely structured clusters. Previous mutational studies, together with our structural observations, indicate that flap-mediated clustering plays an indispensable role in receptor activation.

Based on X-ray crystallographic studies, a globular form of BAFF was proposed to bind BAFFR receptors and activate intracellular signaling by recruiting TRAF3[19,20]. A mutational study targeting the "flap" loop region, which mediates BAFF cage formation, provided support for this hypothesis[22]. However, other studies have challenged this model, as BAFF primarily exists as a trimer in the bloodstream rather than as a cage. Our cryo-EM study demonstrated that both trimeric and cage forms of BAFF form pentagonal clusters with identical structures
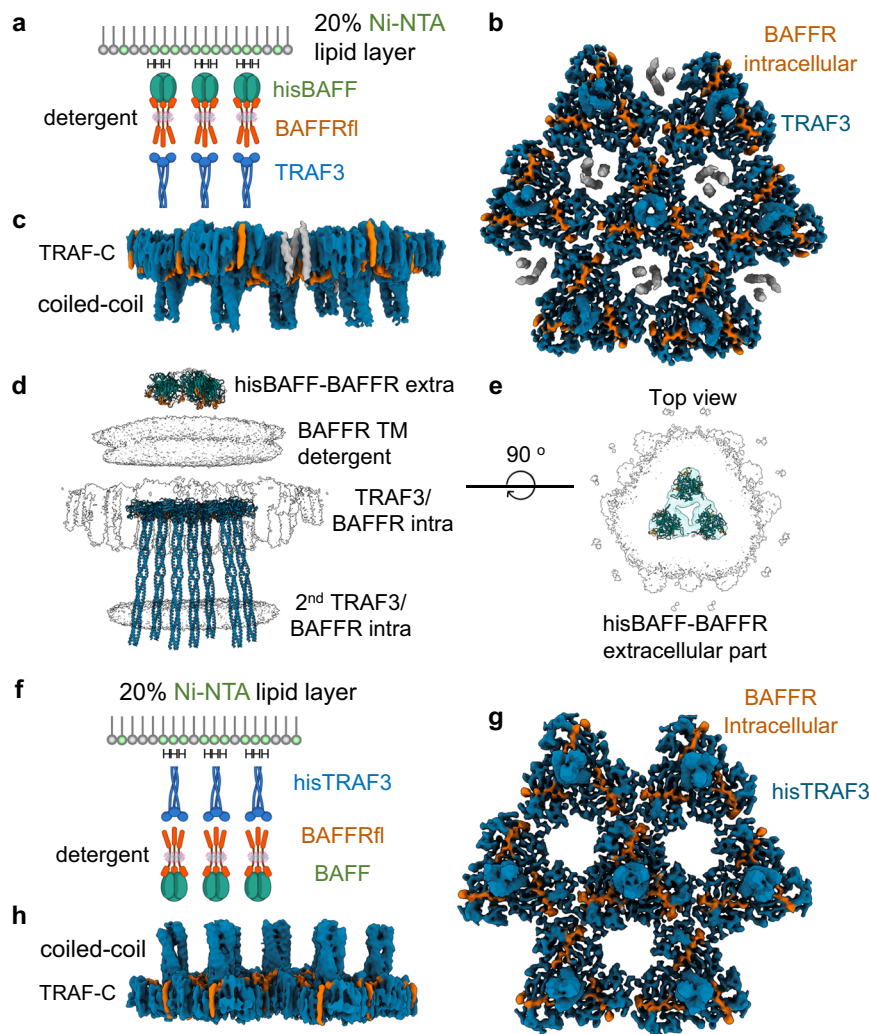
Fig. 8 | Clustered structures of the BAFF-BAFFRfl-TRAF3 complexes. a A hexa-histidine tag was attached to the N-terminus of BAFF, allowing the hisBAFF-BAFFRfl-TRAF3 complex to bind to the Ni-NTA lipid monolayer. The head groups of Ni-NTA lipids are indicated in green. "H" denotes the histidine tag. Created in BioRender. Lim, C. (2025) https://BioRender.com/z6b5t4x. **b** Bottom view and **c** side view of the cryo-EM map of the hisBAFF-BAFFRfl-TRAF3 cluster. The BAFFR intracellular domain and TRAF3 proteins are colored orange and blue, respectively. Alpha helical rods from the second TRAF3 cluster are shown in gray. Focused refinement of the TRAF3 cluster region was performed for 3D map reconstruction. **d** Side view of the cryo-EM map of the hisBAFF-BAFFRfl-TRAF3 cluster without the focused refinement of the TRAF3 region. The structures of BAFF, BAFFR, and TRAF3 are fitted into the map. The map, BAFF, BAFFR, and TRAF3 proteins are shown in gray,

green, orange, and blue, respectively. Due to structural flexibility, only part of the TRAF3 coiled-coil helices are visible. The missing segments of the TRAF3 coiled-coil helices were predicted using AlphaFold3. **e** Top view of the cryo-EM map of the hisBAFF- BAFFRfl-TRAF3 cluster without focused refinement. The map corresponding to the extracellular side of the hisBAFF-BAFFR-TRAF3 cluster is shown in light cyan. The structures of three BAFF-BAFFRecto trimers are fitted into the map. **f** An octa-histidine tag was attached to the N-terminus of TRAF3, allowing the BAFF-BAFFRfl-hisTRAF3 complex to bind to the Ni-NTA lipid monolayer. The head groups of Ni-NTA lipids are indicated in green. "H" denotes the histidine tag. Created in BioRender. Lim, C. (2025) https://BioRender.com/z6b5t4x. **g** Top view and **h** side view of the electron density map of the BAFF-BAFFRfl-hisTRAF3 cluster. The BAFFR intracellular domain and TRAF3 are colored orange and blue, respectively.

upon binding to BAFFR on the membrane. This finding explains why both trimeric and cage forms of BAFF exhibit full biological activity. Strong ionic interactions between the flap regions of BAFF appear to be the primary driving force behind cluster formation and receptor activation. As shown in Fig. 7, mutations in these regions can disrupt cluster formation and inhibit BAFF signaling. The receptors, BAFFR, TACI, and BCMA, are positioned in distant regions of the cluster and do not contribute to cluster formation.

The key mechanism driving the structural transition from the pentagonal BAFF-BAFFR cluster to the hexagonal BAFF-BAFFR-TRAF3 cluster remains unclear. Several factors may influence this shift. First, the clustering interface involving the BAFFR intracellular domain and TRAF3 may play a crucial role in this transition (Fig. 9b). However, this seems unlikely, as interactions between TRAF3 trimers within the cluster appear weak and cannot be reproduced without a bound lipid

layer. Although some amino acid residues of TRAF3 and BAFFR make close contact at the clustering interface, they do not form strong interactions. It cannot provide enough energy to disrupt pentagonal clustering of BAFF in the extracellular side. Instead, the transition to the hexagonal cluster may be necessary to maximize TRAF3 binding to the BAFFR intracellular domain, as the pentagonal cluster cannot accommodate a 1:1 molar ratio of TRAF3 to BAFFR. Future mutational, computational, and structural studies, not only on BAFF but also on other TNF family receptors, are needed to elucidate the role of this structural shift to hexagonal clusters in receptor activation.

The high-resolution structure of the extracellular portion of the BAFF−BAFFR cluster bound to TRAF3 could not be determined. However, the low-resolution map of the extracellular region of the hisBAFF−BAFFRfl−TRAF3 complex within the cluster revealed a partial hexagonal arrangement (Fig. 8e). We propose that the pentagonal
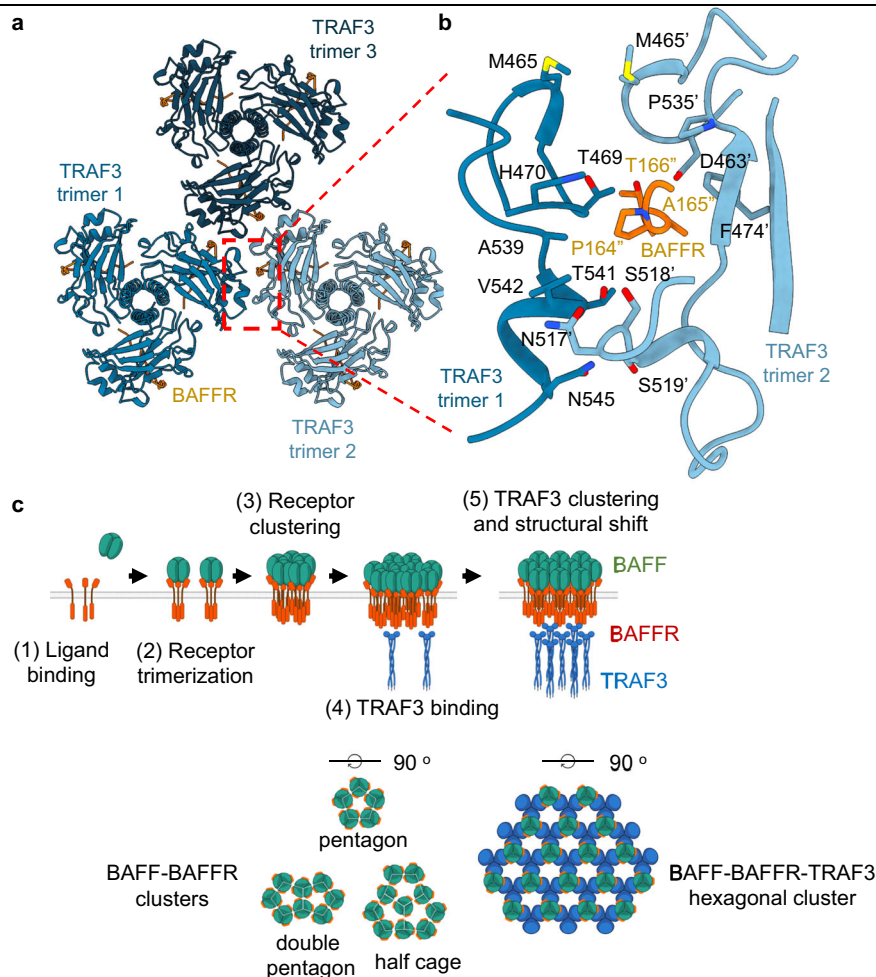
Fig. 9 | Close-up view of the hisBAFF-BAFFR-TRAF3 cluster and the proposed model of BAFFR activation. a Assembly of the three hisBAFF-BAFFRfl-TRAF3 trimers within the cluster is shown. TRAF3 and the BAFFR intracellular domain are colored in a blue gradient and orange, respectively. A clustering interface formed by TRAF3 and the BAFFR intracellular domain is highlighted with a dashed red box and enlarged in (**b**). **b** Close-up view of the clustering interface. Residue numbers for the second TRAF3 trimer are indicated with an apostrophe, while residue numbers for the BAFFR intracellular domain are shown in orange and marked with a double apostrophe. Sulfur, nitrogen, and oxygen atoms in the side chains are colored yellow, blue, and red, respectively. **c** Proposed model for BAFFR activation by BAFF. BAFF, BAFFR, and TRAF3 are shown in green, orange, and blue, respectively. The plasma membrane is schematically drawn in gray. Created in BioRender. Lim, C. (2025) https://BioRender.com/z6b5t4x.

BAFF−BAFFR cluster, characterized by an inter-trimeric angle of 108°, becomes flattened upon TRAF3 binding, enabling the incorporation of additional BAFF−BAFFR−TRAF3 trimeric units. This structural rearrangement results in a hexagonal lattice with an inter-trimeric angle of 120°. We further suggest that the hexagonal extracellular BAFF−BAFFR cluster is more flexible than the pentagonal form due to the increased spacing between trimeric units (Supplementary Fig. 15). This flexibility likely contributes to the observed fading of the electron density map during refinement and resolution enhancement in CryoSPARC software[52].

The simple aggregation of receptors in close proximity without an ordered structure is insufficient to activate TNFR1 and BAFFR. Although the E223K mutation in BAFF disrupts the ordered structure of the cluster, the mutant ligand-receptor complexes can still aggregate, as shown in Fig. 7b, c. Similarly, the binding of the DOM1h nanobody weakens TNFR1 receptor dimerization. However, 40% of TNFR1 receptors on the lipid layer still formed dimers, albeit with a distorted structure (Fig. 3c, d). Therefore, the receptor cluster requires a precise structure to activate TNFR1 and BAFFR signaling pathways. A simple, unstructured aggregation of receptors does not activate the receptor. However, it remains unclear why a cluster with an ordered structure is required for receptor activation and signal initiation. It is

possible that ordered clusters have a higher affinity for signaling adaptors, such as TRAF3 or TRADD. Previous crystallographic studies have shown that the N-terminal zinc finger domains of TRAF2 and 6 dimerize[35,36]. These studies proposed that the dimerization of the TRAF N-terminal domains cross-links the trimeric TRAF C-terminal domains and induces the hexagonal clustering of full-length TRAFs[37]. Thus, this preformed cluster of TRAF3 may have a higher affinity for the pentagonal BAFF-BAFFR cluster. Alternatively, the clustering of TRAF may be necessary for the proper engagement of downstream effectors, such as NIK, TRAF2, and cIAP, among other signaling proteins. Further research is required to clarify the exact roles of the ordered clustering of TNFR1 and BAFFR receptors.

The lipid monolayer appeared to play two roles in TNFR1 and BAFFR clustering. First, it restrains receptors in a viscous two-dimensional layer, which enhances the lateral interaction between protein molecules owing to its favorable entropic effect[53,54]. The protein bound to the 2D lipid layer already has low entropy compared to a freely diffusible protein in a 3D solution space. This reduction in dimensionality favors clustering because the entropy lost by clustering is lower for proteins that are already attached to the lipid layer. Second, the confinement of the protein to the 2D lipid layer limits the shape of the receptor-ligand complexes. For example, previous

crystallographic studies demonstrated that the ectodomain of the BAFFR-BAFF complex forms a large globular cage[19,20]. This structure is evidently impossible when receptors with transmembrane domains are constrained to a flat 2D lipid membrane.

Nineteen of the 29 TNF receptor family proteins engage with various TRAFs, including TRAF2, 3, and 6, when activated by TNF ligand family proteins[3]. Most of the remaining TNF receptors use adaptors containing death domains for signaling. Further research is required to determine whether TRAF family proteins other than TRAF3 and death domain-containing adaptors, including TRADD and FADD, form ordered clusters when bound to ligand-receptor clusters. An extensive body of evidence suggests that higher-order clustering is essential for activating single transmembrane receptors other than the TNF receptor family[55–58]. Furthermore, some GPCRs and ion channels have been proposed to form higher-order complexes[59–63]. However, most of these clusters are unstable when isolated from the membrane environment; consequently, high-resolution structural characterization has been proven difficult. The lipid monolayer method can have broad applications for studying these fragile protein clusters.

One technical challenge associated with the monolayer method is the pronounced anisotropy of cryo-EM data, arising primarily from the relative scarcity of side views. In our data, most of the observed side views originated from contaminating liposomes that spontaneously formed during monolayer generation. This issue can be partially mitigated by tilting the sample stage during data collection, as we did for most of the cryo-EM experiments summarized in Supplementary Figs. 16–31. However, tilted data collection is more time-consuming and often results in lower-quality images compared to untilted data. The anisotropic nature of the images leads to distorted electron density maps, making structural analysis more challenging. Consequently, we believe that the lipid monolayer method is not optimal for the high-resolution determination of initial protein structures. Instead, it is best suited for analyzing the clustering patterns of proteins whose structures in unclustered states have already been determined by other methods or reliably predicted by AlphaFold.

TNF family proteins have been studied for decades, with numerous mutational, biochemical, biophysical, and immunological studies conducted. Many of these studies suggest that TNF receptor family proteins form clusters on the membrane. Here, we demonstrate, for the first time, that the TNF receptor family proteins TNFR1 and BAFFR form highly ordered clusters on lipid membranes upon ligand binding. We also show that a non-competitive inhibitor or inactivating mutations in the ligands disrupt the precise structural organization of these receptor-ligand clusters. We propose that other TNF family receptors may function through similar mechanisms. Structural studies of receptor-ligand clusters could facilitate the discovery of therapeutic agents capable of regulating receptor activity by modulating their clustered structures.

Methods

Gene cloning and protein expression
For full-length human TNFR1 and BAFFR, the genes encoding the proteins with various tags were synthesized (Twist Bioscience) and cloned into the pEG BacMam baculovirus transfer vector (Supplementary Tables 1 and 4)[64]. The plasmid was transformed into DH10Bac *E. coli* for transposition into the bacmid[64]. Recombinant baculovirus was generated by transfecting Sf9 insect cells with the bacmid DNA. Protein expression was conducted in HEK293 GnTI⁻ cells cultured in FreeStyle 293 medium (Thermo Fisher), supplemented with 1% (v/v) fetal bovine serum (Sigma-Aldrich), in a 10% CO_2 shaking incubator. The cells were infected with 8% (v/v) baculovirus at a density of 3×10^6 cells per ml. Protein expression was enhanced by adding 10 mM sodium butyrate (Sigma-Aldrich) 12–16 h post-infection, followed by incubation for an additional 48–60 h. The cells were collected by

centrifugation at $7261 \times g$ for 30 min, flash-frozen in liquid nitrogen, and stored at −80 °C.

Genes other than the TNFR1fl and BAFFRfl were synthesized (Twist Bioscience) and cloned into the pAcGP67A or pVL1393 baculovirus transfer vectors (BD Biosciences) (Supplementary Tables 1 and 4). Recombinant baculovirus was generated by co-transfecting Sf9 insect cells with a linearized baculovirus genome, BestBac2.0 (Expression Systems). Protein expression was carried out in High Five insect cells cultured in ESF 921 medium (Expression Systems) by adding 4% (v/v) baculovirus and incubating at 27 °C for 72 h.

Purification of the wild type and the mutant of BAFF
The secreted protein was bound to cOmplete His-Tag Purification Resin (Roche) and eluted using an elution buffer containing 20 mM Tris-HCl, 150 mM NaCl, and 300 mM imidazole, pH 7.8. The histidine tag was removed by incubation with thrombin at 4 °C for 16 h. The cleaved protein was purified without concentration using a Superdex 200 Increase 10/300 GL gel filtration column (Cytiva) equilibrated with a buffer containing 20 mM Tris-HCl and 150 mM NaCl (pH 7.8). Fractions corresponding to the molecular weight of trimeric BAFF were collected (Supplementary Fig. 10a). For the purification of the cage form of BAFF, the cleaved protein was concentrated to more than 1.5 mg/ml using an ultrafiltration membrane that has a molecular weight cutoff of 50 kDa. The protein was then purified using a Superdex 200 Increase 10/300 GL gel filtration column (Cytiva) equilibrated with a buffer containing 20 mM Tris-HCl and 150 mM NaCl, pH 7.8. Fractions corresponding to the BAFF cage were collected.

Purification of TNFα, TNFR1ecto, BAFFRecto, BCMAecto, TACIecto, TRAF3, hisTRAF3 and DOM1h from insect cells
For soluble TNFα, TNFR1ecto, BAFFRecto, BCMAecto, TACIecto, and DOM1h nanobody, the secreted proteins were bound to cOmplete His-Tag Purification resin (Roche) and eluted using an elution buffer containing 20 mM Tris-HCl, 150 mM NaCl, and 300 mM imidazole, pH 7.8. The proteins were further purified using a Superdex 200 Increase 10/300 GL gel filtration column (Cytiva) equilibrated with a buffer containing 20 mM Tris-HCl and 150 mM NaCl, pH 7.8. For TNFα without the histidine tag, the histidine tag was removed by thrombin treatment at 4 °C for 16 h, followed by another round of gel filtration chromatography. The solution was then passed through the cOmplete His-Tag Purification column to remove uncleaved protein.

For TRAF3 and hisTRAF3, a frozen aliquot of the insect cells infected by the recombinant baculoviruses was thawed and resuspended in a buffer containing 20 mM Tris-HCl, pH 8.0, 150 mM NaCl, and 0.5 mM phenylmethylsulfonyl fluoride (PMSF). The cells were lysed using a microfluidizer (Microfluidics), and the protein was bound to cOmplete His-Tag Purification resin (Roche). Elution was performed using a buffer containing 20 mM Tris-HCl, 150 mM NaCl, and 300 mM imidazole, pH 7.8. The protein was further purified using a Superdex 200 Increase 10/300 GL gel filtration column (Cytiva) equilibrated with a buffer containing 20 mM Tris-HCl and 150 mM NaCl, pH 7.8. For TRAF3 purification without the histidine tag, the protein eluted from the cOmplete His-Tag Purification resin was treated with thrombin at 4 °C for 16 h, followed by Superdex 200 gel filtration chromatography. The protein-containing fractions were collected and passed through the cOmplete His-Tag Purification column to remove uncleaved protein.

Purification of the full-length TNFR1 and BAFFR from HEK293 cells
For the purification of full-length BAFFR and TNFR1, a frozen aliquot of cells was thawed and resuspended in a lysis buffer containing 20 mM Tris-HCl, pH 8.0, 150 mM NaCl, 0.5 mM PMSF, 1 mM benzamidine chloride, 1 μg/ml leupeptin, 1 μg/ml aprotinin, and 1 μg/ml pepstatin. The cells were lysed using a homogenizer, and the membrane fraction

was collected by ultracentrifugation at 200,000×*g* for one hour. The resulting pellet was resuspended in lysis buffer, and membrane solubilization was performed by adding 1% (w/v) Fos-Choline-14 (FC-14, Anatrace), followed by incubation at 4 °C for 1 h with gentle rotation. For BAFFR, the membrane fraction was incubated with its ligand by adding 16 µg/ml of BAFF and gently rotating at 4 °C for 1.5 h. Following FC-14 extraction, insoluble fractions were removed by ultracentrifugation at 200,000×*g* for one hour. The supernatant was loaded onto a column packed with agarose resin conjugated to an anti-ALFA nanobody[65]. After protein binding, the column was washed with 40 column volumes of wash buffer containing 20 mM Tris-HCl, pH 8.0, 150 mM NaCl, and 0.005% FC-14. Protein was eluted by treatment with 1% PreScission protease (Cytiva) overnight. The eluted protein solution was then concentrated using an ultracentrifugal filter with a 50 kDa cutoff (Merck Millipore).

Preparation of the lipid monolayer

The lipid monolayer was prepared as previously described[41]. Briefly, a Teflon block with an 85 µl well and a side injection tunnel was used (Supplementary Fig. 1a). The wells were washed with ethanol and distilled water. The Teflon block was then placed in a humid environment inside a Petri dish containing wet filter paper. Each well was filled with 65 µl of buffer containing 20 mM Tris-HCl and 150 mM NaCl, pH 7.8. Next, 1 µl of a lipid solution containing 0.8 mg/ml POPC (Sigma) and 0.2 mg/ml DGS-NTA(Ni^{2+}) (Sigma) dissolved in chloroform was gently added on top of the buffer. The Teflon block was left undisturbed in the Petri dish at room temperature for 30 min to allow chloroform evaporation. The lipid monolayer formed spontaneously.

Preparation of cryo-EM grids for the TNFα-TNFR1ecto, TNFα-TNFR1fl, BAFF-BAFFRecto, BAFF-BAFFRfl, BAFF-BCMAecto and BAFF-TACIecto complexes

For cryo-EM grid preparation, 20 µl of a solution containing the receptor-ligand complex was injected into the side tunnel of the lipid monolayer well. The protein solution in the well was then gently mixed using a pipette inserted into the side tunnel and incubated at room temperature for 2 h to allow the histidine-tagged protein to bind to the lipid monolayer. Next, a Quantifoil 1.2/1.3 gold EM grid (Quantifoil Micro Tools), with the carbon side facing downward, was placed on top of the well and left undisturbed for 30 min to allow the lipid layer to adhere to the carbon film. Subsequently, 15 µl of buffer was added to the side tunnel of the well. The grid was then gently picked up with forceps and plunge-frozen using a Vitrobot Mark IV (Thermo Fisher Scientific) at 18 °C and 100% humidity, with no applied force, after 6 sec of blotting.

Preparation of cryo-EM grids for the hisBAFF-BAFFRfl-TRAF3 complex

For cryo-EM grid preparation, 20 µl of buffer was removed from the side tunnel of the Teflon well, and 20 µl of 0.1 mg/ml full-length BAFFR in complex with hexa-histidine-tagged BAFF was added. The solution was gently mixed using a pipette and incubated at room temperature for two hours. To reduce the concentration of unbound protein in the well, 30 µl of the protein solution was replaced twice with 30 µl of buffer solution. Next, 30 µl of 0.2 mg/ml TRAF3, lacking the hexa-histidine tag, was added to the side tunnel and incubated at room temperature for five hours. A Quantifoil 1.2/1.3 gold EM grid (Quantifoil Micro Tools), with the carbon side facing downward, was placed on top of the Teflon well and left undisturbed for 30 min to allow the lipid layer to adhere to the carbon film. Subsequently, 15 µl of buffer was added to the side tunnel of the well. The grid was then gently picked up with forceps and plunge-frozen using a Vitrobot Mark IV (Thermo Fisher Scientific) at 18 °C and 100% humidity, with no applied force, after 6 sec of blotting.

Preparation of cryo-EM grids for the BAFF-BAFFRfl-hisTRAF3 complex

For cryo-EM grid preparation, 20 µl of buffer was removed from the Teflon well, and 20 µl of 0.1 mg/ml hisTRAF3 with an N-terminal octa-histidine tag was added. The solution was gently mixed using a pipette and incubated at room temperature for two hours. To reduce the concentration of unbound protein in the well, 30 µl of the protein solution in the well was replaced twice with 30 µl of buffer solution. Next, 30 µl of 0.2 mg/ml full-length BAFFR in complex with BAFF, lacking the hexa-histidine tag, was added to the side tunnel of the well and incubated at room temperature for five hours. A Quantifoil 1.2/1.3 gold EM grid (Quantifoil Micro Tools), with the carbon side facing downward, was placed on top of the Teflon well and left undisturbed for 30 min to allow the lipid layer to adhere to the carbon film. Subsequently, 15 µl of buffer was added to the side tunnel of the well. The grid was then gently picked up with forceps and plunge-frozen using a Vitrobot Mark IV (Thermo Fisher Scientific) at 18 °C and 100% humidity, with no applied force, after 6 s of blotting.

Preparation of cryo-EM grids for the TNFα-TNFR1ecto-DOM1h complex

TNFα, TNFR1ecto, and DOM1h proteins were mixed in a 1:1.3:1.5 molar ratio to prepare the protein complex, with a total protein concentration of 1.1 mg/ml. To reduce the orientation preference of protein particles on the cryo-EM grids, 0.00021% glycol-diosgenin (GDN) detergent was added to the buffer solution. For grid preparation, 300-mesh Quantifoil R 1.2/1.3 copper EM grids (Quantifoil Micro Tools) were glow-discharged at 15 mA for 60 s using a glow-discharger (PELCO). Cryo-EM grid samples were then prepared using a Vitrobot Mark IV (Thermo Fisher Scientific) at 4 °C and 100% humidity. A 3.5-µl aliquot of the sample was applied to the cryo-EM grid and blotted for 5 s before plunge-freezing. The preparation of cryo-EM grids for the TNFα-TNFR1ecto-DOM1h complex bound to the lipid monolayer was performed as described in the previous section.

Cryo-EM data collection and processing

The data collection statistics are summarized in Supplementary Tables 2 and 3, and 5–8. All cryo-EM data processing was performed using CryoSPARC v4.4.1[52] at the Institute of Membrane Proteins (NFEC-2025-03-304437) and is summarized in Supplementary Figs. 16–31. Briefly, cryo-EM movie files were preprocessed using patch motion correction and patch contrast transfer function (CTF) estimation. Poor-quality micrographs were manually curated based on CTF estimations, ice thickness, and total frame motion. Initial particle selection was performed using the blob-picking method, followed by purification through 2D classification. High-quality 2D class averages were selected to generate a Topaz particle-picking model[66]. The particle-picking process was further optimized by performing 2–3 rounds of Topaz analysis and multiple rounds of 2D classification. The initial model was generated using ab initio reconstruction or by fitting known protein structures into the map. The electron density map was refined through homogeneous and non-uniform refinement. The final map was obtained by un-binning the particles and performing non-uniform refinement. The map was then sharpened, and noise was reduced using DeepEMhancer, an automated deep learning-based sharpening method[67].

For the TNFα-TNFR1ecto-DOM1h complex, the CRD4 domain of TNFR1ecto and the DOM1h nanobody could not be resolved in the electron density map due to the high flexibility and independent motion of these domains. To address this issue, a focused refinement was performed to improve the resolution of the CRD4 and nanobody regions (Supplementary Fig. 22). Signal contributions from the two CRD4 domains and their bound nanobodies were subtracted using the particle subtraction method. The map for the remaining CRD4 domain and nanobody was further improved through local refinement with a

mask covering the trimeric TNFα ligands and a single TNFR1ecto bound to the nanobody. After model building, a composite map reproducing C3 symmetry and encompassing all three nanobodies was generated using the "Combine Focus Maps" function in the program Phenix[68].

Model building

The initial structural templates for the binary cluster of the TNFα-TNFR1ecto complex were obtained from crystallographic structures of TNFα (PDB ID: 7KPB)[69] and TNFR1ecto (PDB ID: 7KP7)[8]. These initial models were fitted into the cryo-EM density map using ChimeraX[70]. The resulting structure of the binary cluster of the TNFα-TNFR1ecto complex was refined through multiple rounds of model building using Coot and Phenix[68,71]. The bent, trigonal, and linear quadruple clusters of the TNFα-TNFR1ecto complex, as well as the binary cluster of the TNFα-TNFR1fl complex, were modeled by rigid-body fitting of the trimeric TNFα-TNFR1ecto structure into the density map. The TNFα-TNFR1ecto-DOM1h complex was modeled using a similar approach. The initial model for the DOM1h nanobody was generated using AlphaFold 3[72].

The initial model for the pentagonal cluster of the BAFF-BAFFRecto complex was obtained by rigid-body fitting of the pentagonal substructure extracted from the crystal structure of the BAFF-BAFFRecto cage (PDB ID: 4V46). The resulting model was refined through multiple rounds of model building using Coot and Phenix with reference model restraints. The structures of the double pentagonal and half-spherical clusters of the BAFF-BAFFRecto complex, as well as the pentagonal cluster of the BAFF-BAFFRfl complex, were initially built by rigid-body fitting of the trimeric BAFF-BAFFRecto complex and refined using a similar method.

The initial model for the hisBAFF-BAFFRfl-TRAF3 complex was generated by combining previously reported structures of TRAF3 (PDB ID: 8T5P)[73] and the BAFFR intracellular domain (PDB ID: 2GKW)[27]. The model was refined through iterative model-building steps using Coot and Phenix. The reported crystal structure of TRAF3 contains a shorter coiled-coil domain than the TRAF3 protein used in the cryo-EM study. The missing portion of the coiled-coil α-helix was extracted from a TRAF3 model predicted by AlphaFold 3[72]. The refinement statistics are summarized in Supplementary Tables 2, 5, and 8. All figures displaying electron density maps, structural analyses, and representations were generated using ChimeraX and Coot[70,71].

Reporting summary

Further information on research design is available in the Nature Portfolio Reporting Summary linked to this article.

Data availability

The cryo-EM maps and the atomic coordinates were deposited in the Electron Microscopy Data Bank (EMDB) and the Protein Data Bank (PDB), respectively, under the following accession codes: EMD-60484 and 8ZUI for the TNFα-TNFR1ecto binary cluster; EMD-60489 for the bent cluster; EMD-60497 for the trigonal cluster; EMD-60491 for the linear quadruple cluster; EMD-63627 for the quintuple cluster; EMD-60490 for the TNFα-TNFR1fl binary cluster; EMD-60549 for the TNFα-TNFR1ecto-DOM1h complex in the solution state; EMD-60494 for the TNFα-TNFR1ecto-DOM1h binary cluster; EMD-60485 and 8ZUJ for the BAFF-BAFFRecto pentagonal cluster; EMD-60492 for the double pentagonal cluster; EMD-60493 for the half sphere cluster; EMD-60487 for the BAFF-BAFFRfl pentagonal cluster; EMD-63178 for the BAFF-BCMAecto cluster; EMD-63177 for the BAFF-TACIecto cluster; EMD-60486 and 8ZUK for the hisBAFF-BAFFRfl-TRAF3 cluster; EMD-60488 for the BAFF-BAFFRfl-hisTRAF3 cluster. Source data are provided with this paper.

References

1. Kucka, K. & Wajant, H. Receptor oligomerization and its relevance for signaling by receptors of the tumor necrosis factor receptor superfamily. *Front. Cell Dev. Biol.* **8**, 615141 (2020).
2. Dostert, C., Grusdat, M., Letellier, E. & Brenner, D. The TNF family of ligands and receptors: communication modules in the immune system and beyond. *Physiol. Rev.* **99**, 115–160 (2019).
3. Wallach, D. The tumor necrosis factor family: family conventions and private idiosyncrasies. *Cold Spring Harb. Perspect. Biol.* **10**, a028431 (2018).
4. Croft, M., Benedict, C. A. & Ware, C. F. Clinical targeting of the TNF and TNFR superfamilies. *Nat. Rev. Drug Discov.* **12**, 147–168 (2013).
5. Abitbol, V., Benkhalifa, S., Habauzit, C. & Marotte, H. Navigating adalimumab biosimilars: an expert opinion. *J. Comp. Eff. Res.* **12**, e230117 (2023).
6. Yang, S., Wang, J., Brand, D. D. & Zheng, S. G. Role of TNF-TNF receptor 2 signal in regulatory T cells and its therapeutic implications. *Front. Immunol.* **9**, 784 (2018).
7. Banner, D. W. et al. Crystal structure of the soluble human 55 kd TNF receptor-human TNF beta complex: implications for TNF receptor activation. *Cell* **73**, 431–445 (1993).
8. McMillan, D. et al. Structural insights into the disruption of TNF-TNFR1 signalling by small molecules stabilising a distorted TNF. *Nat. Commun.* **12**, 582 (2021).
9. Naismith, J. H. & Sprang, S. R. Modularity in the TNF-receptor family. *Trends Biochem. Sci.* **23**, 74–79 (1998).
10. Hsu, H., Xiong, J. & Goeddel, D. V. The TNF receptor 1-associated protein TRADD signals cell death and NF-kappa B activation. *Cell* **81**, 495–504 (1995).
11. Li, Z., Yuan, W. & Lin, Z. Functional roles in cell signaling of adaptor protein TRADD from a structural perspective. *Comput. Struct. Biotechnol. J.* **18**, 2867–2876 (2020).
12. Siegmund, D., Wagner, J. & Wajant, H. TNF receptor associated factor 2 (TRAF2) signaling in cancer. *Cancers (Basel)* **14**, 4055 (2022).
13. Rothe, M., Wong, S. C., Henzel, W. J. & Goeddel, D. V. A novel family of putative signal transducers associated with the cytoplasmic domain of the 75 kDa tumor necrosis factor receptor. *Cell* **78**, 681–692 (1994).
14. Mukai, Y. et al. Solution of the structure of the TNF-TNFR2 complex. *Sci. Signal.* **3**, ra83 (2010).
15. Schweighoffer, E. & Tybulewicz, V. L. BAFF signaling in health and disease. *Curr. Opin. Immunol.* **71**, 124–131 (2021).
16. Smulski, C. R. & Eibel, H. BAFF and BAFF-receptor in B cell selection and survival. *Front. Immunol.* **9**, 2285 (2018).
17. Ullah, M. A. & Mackay, F. The BAFF-APRIL system in cancer. *Cancers (Basel)* **15**, 1791 (2023).
18. Samy, E., Wax, S., Huard, B., Hess, H. & Schneider, P. Targeting BAFF and APRIL in systemic lupus erythematosus and other antibody-associated diseases. *Int. Rev. Immunol.* **36**, 3–19 (2017).
19. Kim, H. M. et al. Crystal structure of the BAFF-BAFF-R complex and its implications for receptor activation. *Nat. Struct. Biol.* **10**, 342–348 (2003).
20. Liu, Y. et al. Ligand-receptor binding revealed by the TNF family member TALL-1. *Nature* **423**, 49–56 (2003).
21. Liu, Y. et al. Crystal structure of sTALL-1 reveals a virus-like assembly of TNF family ligands. *Cell* **108**, 383–394 (2002).
22. Vigolo, M. et al. A loop region of BAFF controls B cell survival and regulates recognition by different inhibitors. *Nat. Commun.* **9**, 1199 (2018).
23. Moore, P. A. et al. BLyS: member of the tumor necrosis factor family and B lymphocyte stimulator. *Science* **285**, 260–263 (1999).
24. Schneider, P. et al. BAFF, a novel ligand of the tumor necrosis factor family, stimulates B cell growth. *J. Exp. Med.* **189**, 1747–1756 (1999).

25. Shu, H. B., Hu, W. H. & Johnson, H. TALL-1 is a novel member of the TNF family that is down-regulated by mitogens. *J. Leukoc. Biol.* **65**, 680–683 (1999).

26. Gardam, S., Sierro, F., Basten, A., Mackay, F. & Brink, R. TRAF2 and TRAF3 signal adapters act cooperatively to control the maturation and survival signals delivered to B cells by the BAFF receptor. *Immunity* **28**, 391–401 (2008).

27. Ni, C. Z. et al. Key molecular contacts promote recognition of the BAFF receptor by TNF receptor-associated factor 3: implications for intracellular signaling regulation. *J. Immunol.* **173**, 7394–7400 (2004).

28. Xu, L. G. & Shu, H. B. TNFR-associated factor-3 is associated with BAFF-R and negatively regulates BAFF-R-mediated NF-kappa B activation and IL-10 production. *J. Immunol.* **169**, 6883–6889 (2002).

29. So, T. The immunological significance of tumor necrosis factor receptor-associated factors (TRAFs). *Int. Immunol.* **34**, 7–20 (2022).

30. Ha, H., Han, D. & Choi, Y. TRAF-mediated TNFR-family signaling. *Curr. Protoc. Immunol.* **11**, 19D 11–11 19D 19 (2009).

31. Park, H. H. Structure of TRAF family: current understanding of receptor recognition. *Front. Immunol.* **9**, 1999 (2018).

32. Ni, C. Z. et al. Molecular basis for CD40 signaling mediated by TRAF3. *Proc. Natl. Acad. Sci. USA* **97**, 10395–10399 (2000).

33. McWhirter, S. M. et al. Crystallographic analysis of CD40 recognition and signaling by human TRAF2. *Proc. Natl. Acad. Sci. USA* **96**, 8408–8413 (1999).

34. Ye, H., Park, Y. C., Kreishman, M., Kieff, E. & Wu, H. The structural basis for the recognition of diverse receptor sequences by TRAF2. *Mol. Cell* **4**, 321–330 (1999).

35. Yin, Q. et al. E2 interaction and dimerization in the crystal structure of TRAF6. *Nat. Struct. Mol. Biol.* **16**, 658–666 (2009).

36. Yin, Q., Lamothe, B., Darnay, B. G. & Wu, H. Structural basis for the lack of E2 interaction in the RING domain of TRAF2. *Biochemistry* **48**, 10558–10567 (2009).

37. Vanamee, E. S. & Faustman, D. L. Structural principles of tumor necrosis factor superfamily signaling. *Sci. Signal.* **11**, eaao4910 (2018).

38. Idriss, H. T. & Naismith, J. H. TNF alpha and the TNF receptor superfamily: structure-function relationship(s). *Microsc. Res. Tech.* **50**, 184–195 (2000).

39. Naismith, J. H., Devine, T. Q., Brandhuber, B. J. & Sprang, S. R. Crystallographic evidence for dimerization of unliganded tumor necrosis factor receptor. *J. Biol. Chem.* **270**, 13303–13307 (1995).

40. Karathanasis, C. et al. Single-molecule imaging reveals the oligomeric state of functional TNFalpha-induced plasma membrane TNFR1 clusters in cells. *Sci. Signal.* **13**, eaax5647 (2020).

41. Truong, C. D., Williams, D. R., Zhu, M., Wang, J. C. & Chiu, P. L. Sample preparation using a lipid monolayer method for electron crystallographic studies. *J. Vis. Exp.* **177**, e63015 (2021).

42. Kelly, D. F., Dukovski, D. & Walz, T. A practical guide to the use of monolayer purification and affinity grids. *Methods Enzymol.* **481**, 83–107 (2010).

43. Dufourc, E. J. Bicelles and nanodiscs for biophysical chemistry. *Biochim. Biophys. Acta Biomembr.* **1863**, 183478 (2021).

44. Chan, F. K. et al. A domain in TNF receptors that mediates ligand-independent receptor assembly and signaling. *Science* **288**, 2351–2354 (2000).

45. Enever, C., Pupecka-Swider, M. & Sepp, A. Stress selections on domain antibodies: 'what doesn't kill you makes you stronger'. *Protein Eng. Des. Sel.* **28**, 59–66 (2015).

46. Fairclough, L. C. et al. Tumour necrosis factor receptor I blockade shows that TNF-dependent and TNF-independent mechanisms synergise in TNF receptor associated periodic syndrome. *Eur. J. Immunol.* **45**, 2937–2944 (2015).

47. Schmidt, E. M. et al. Selective blockade of tumor necrosis factor receptor I inhibits proinflammatory cytokine and chemokine production in human rheumatoid arthritis synovial membrane cell cultures. *Arthritis Rheum.* **65**, 2262–2273 (2013).

48. Espirito Santo, A. I. et al. Selective inhibition of TNFR1 reduces osteoclast numbers and is differentiated from anti-TNF in a LPS-driven model of inflammatory bone loss. *Biochem. Biophys. Res. Commun.* **464**, 1145–1150 (2015).

49. Thil Dinuk Batuwangala, A. S., Armin Sepp & Adriaan Allart Stoop. Tumor Necrosis Factor Receptor 1 antagonists. United States patent US20140112929A1 (2014).

50. Eslami, M. & Schneider, P. Function, occurrence and inhibition of different forms of BAFF. *Curr. Opin. Immunol.* **71**, 75–80 (2021).

51. Cachero, T. G. et al. Formation of virus-like clusters is an intrinsic property of the tumor necrosis factor family member BAFF (B cell activating factor). *Biochemistry* **45**, 2006–2013 (2006).

52. Punjani, A., Rubinstein, J. L., Fleet, D. J. & Brubaker, M. A. cryoSPARC: algorithms for rapid unsupervised cryo-EM structure determination. *Nat. Methods* **14**, 290–296 (2017).

53. Bray, D. Signaling complexes: biophysical constraints on intracellular communication. *Annu. Rev. Biophys. Biomol. Struct.* **27**, 59–75 (1998).

54. Cebecauer, M., Spitaler, M., Serge, A. & Magee, A. I. Signalling complexes and clusters: functional advantages and methodological hurdles. *J. Cell Sci.* **123**, 309–320 (2010).

55. Lim, C. S. et al. TLR3 forms a highly organized cluster when bound to a poly(I:C) RNA ligand. *Nat. Commun.* **13**, 6876 (2022).

56. Lin, S. C., Lo, Y. C. & Wu, H. Helical assembly in the MyD88-IRAK4-IRAK2 complex in TLR/IL-1R signalling. *Nature* **465**, 885–890 (2010).

57. Li, M. & Yu, Y. Innate immune receptor clustering and its role in immune regulation. *J. Cell Sci.* **134**, jcs249318 (2021).

58. Iwamoto, D. V. & Calderwood, D. A. Regulation of integrin-mediated adhesions. *Curr. Opin. Cell Biol.* **36**, 41–47 (2015).

59. Maurice, P., Kamal, M. & Jockers, R. Asymmetry of GPCR oligomers supports their functional relevance. *Trends Pharmacol. Sci.* **32**, 514–520 (2011).

60. Nemoto, W. & Saito, A. Interface prediction for GPCR oligomerization between transmembrane helices. *Methods Mol. Biol.* **2315**, 99–110 (2021).

61. Choi, K. H. Cooperative gating between ion channels. *Gen. Physiol. Biophys.* **33**, 1–12 (2014).

62. Albizu, L. et al. Time-resolved FRET between GPCR ligands reveals oligomers in native tissues. *Nat. Chem. Biol.* **6**, 587–594 (2010).

63. Fanelli, F., Hanyaloglu, A. C. & Jonas, K. Integrated structural modeling and super-resolution imaging resolve GPCR oligomers. *Prog. Mol. Biol. Transl. Sci.* **169**, 151–179 (2020).

64. Goehring, A. et al. Screening and large-scale expression of membrane proteins in mammalian cells for structural studies. *Nat. Protoc.* **9**, 2574–2585 (2014).

65. Gotzke, H. et al. The ALFA-tag is a highly versatile tool for nanobody-based bioscience applications. *Nat. Commun.* **10**, 4403 (2019).

66. Bepler, T. et al. Positive-unlabeled convolutional neural networks for particle picking in cryo-electron micrographs. *Nat. Methods* **16**, 1153–1160 (2019).

67. Sanchez-Garcia, R. et al. DeepEMhancer: a deep learning solution for cryo-EM volume post-processing. *Commun. Biol.* **4**, 874 (2021).

68. Liebschner, D. et al. Macromolecular structure determination using X-rays, neutrons and electrons: recent developments in Phenix. *Acta Crystallogr. D Struct. Biol.* **75**, 861–877 (2019).

69. Lightwood, D. J. et al. A conformation-selective monoclonal antibody against a small molecule-stabilised signalling-deficient form of TNF. *Nat. Commun.* **12**, 583 (2021).

70. Meng, E. C. et al. UCSF ChimeraX: Tools for structure building and analysis. *Protein Sci.* **32**, e4792 (2023).

71. Emsley, P., Lohkamp, B., Scott, W. G. & Cowtan, K. Features and development of Coot. *Acta Crystallogr. D Biol. Crystallogr.* **66**, 486–501 (2010).
72. Abramson, J. et al. Accurate structure prediction of biomolecular interactions with AlphaFold 3. *Nature* **630**, 493–500 (2024).
73. Busscher, B. M., Befekadu, H. B., Liu, Z. & Xiao, T. S. SARS-CoV-2 ORF3a-mediated NF-kappaB activation is not dependent on TRAF-binding sequence. *Viruses* **15**, 2229 (2023).

Acknowledgements

Author contributions

J-O.L. conceived of and supervised the project. C.S.L. expressed and purified the protein, prepared the sample for the cryo-EM study, collected and processed cryo-EM data, and built and refined the atomic models. J.L. conducted all experiments associated with the DOM1h nanobody. C.S.L., J.W.K., and J-O.L. prepared and edited the manuscript with input from all the authors.

Competing interests

The authors declare no competing interests.

Additional information

Supplementary information The online version contains supplementary material available at https://doi.org/10.1038/s41467-025-61271-6.

Correspondence and requests for materials should be addressed to Jie-Oh Lee.

Peer review information *Nature Communications* thanks Jie Yang and the other, anonymous, reviewer(s) for their contribution to the peer review of this work. A peer review file is available.

Reprints and permissions information is available at http://www.nature.com/reprints

Publisher's note Springer Nature remains neutral with regard to jurisdictional claims in published maps and institutional affiliations.